

**MODELING SEMICONDUCTOR AND
QUARTZ CRYSTAL GROWTH**

FINAL REPORT

EOARD CONTRACT F61708-98-W0015

SPC 98-4001

**STEFAN BALINT
DEPARTMENT OF MATHEMATICS
STATE UNIVERSITY OF THE WEST TIMISOARA
BD. VASILE PARVAN NO. 4
1900 TIMISOARA, ROMANIA**

DECEMBER 1998

19990115 057

AQF99-04-0627

REPORT DOCUMENTATION PAGE

Form Approved OMB No. 0704-0188

Public reporting burden for this collection of information is estimated to average 1 hour per response, including the time for reviewing instructions, searching existing data sources, gathering and maintaining the data needed, and completing and reviewing the collection of information. Send comments regarding this burden estimate or any other aspect of this collection of information, including suggestions for reducing this burden to Washington Headquarters Services, Directorate for Information Operations and Reports, 1215 Jefferson Davis Highway, Suite 1204, Arlington, VA 22202-4302, and to the Office of Management and Budget, Paperwork Reduction Project (0704-0188), Washington, DC 20503.

1. AGENCY USE ONLY (Leave blank)		2. REPORT DATE December 1998	3. REPORT TYPE AND DATES COVERED Final Report	
4. TITLE AND SUBTITLE Modeling Semiconductor and Quartz Crystal Growth			5. FUNDING NUMBERS F617089W0015	
6. AUTHOR(S) Prof Stefan Balint				
7. PERFORMING ORGANIZATION NAME(S) AND ADDRESS(ES) West University of Timisoara Bd. Vasile Parvan no. 4 Timisoara 1900 Romania			8. PERFORMING ORGANIZATION REPORT NUMBER N/A	
9. SPONSORING/MONITORING AGENCY NAME(S) AND ADDRESS(ES) EOARD PSC 802 BOX 14 FPO 09499-0200			10. SPONSORING/MONITORING AGENCY REPORT NUMBER SPC 98-4001	
11. SUPPLEMENTARY NOTES				
12a. DISTRIBUTION/AVAILABILITY STATEMENT Approved for public release; distribution is unlimited.			12b. DISTRIBUTION CODE A	
13. ABSTRACT (Maximum 200 words) This report results from a contract tasking West University of Timisoara as follows: The contractor will investigate an improved mathematical model of mass and heat transport by convection and diffusion during semiconductor crystal growth utilizing the Bridgman-Stockbarger and hydrothermal methods.				
14. SUBJECT TERMS EOARD, Bridgman-Stockbarger Growth, Crystal Growth, Semiconductors			15. NUMBER OF PAGES 52	
			16. PRICE CODE N/A	
17. SECURITY CLASSIFICATION OF REPORT UNCLASSIFIED	18. SECURITY CLASSIFICATION OF THIS PAGE UNCLASSIFIED	19. SECURITY CLASSIFICATION OF ABSTRACT UNCLASSIFIED	20. LIMITATION OF ABSTRACT UL	

NSN 7540-01-280-5500

Standard Form 298 (Rev. 2-89)
Prescribed by ANSI Std. Z39-18
298-102

Preface

This final report concerning modeling semiconductor and quartz crystal growth is focused on the transport equation of the dopant and of the nutrient in neighborhood of the melt/solid and liquid/solid interface.

We present the weakness of the "stagnant-film" or "diffusion-layer" model and using recent developments in the field of periodic material modeling we identify new transport equation in the region adjacent to the interface. This equation takes into account the interaction between complicated global flow patterns and the convective-diffusive dispersion mechanism, which exist in the so-called "mushy zone" or "precrySTALLIZATION region". We assume that in this zone we have a periodic structure, which is a weak form of the periodic structure of the crystal. If the periodic structure in the precrySTALLIZATION region is no significant i.e. the size of the periodically distributed solid inclusions, which are small with respect to the distance between two neighbouring inclusions, is smaller than a critical size; then global flow is not influenced and the transport equation of the solute is the classical convective-diffusive equation except the diffusive term which is more refined because a diffusion tensor appears. But if the periodic structure in the precrySTALLIZATION region is significant i.e. the size of the periodically distributed inclusions is greater than a critical size; then the flow in mushy zone is a Darcy flow and in the new transport equation of the solute we have new more refined convective, diffusive terms. It must be noted that these new equations do not take into account the interaction of the dopant field with the crystal. A kind of interaction appears just in boundary conditions. In this context we can think to improve our equations by the addition of a new term, which expresses this interaction.

Concerning the accuracy of our equations we want to point out that we have established a convergence result, which proves that our equations obtained by homogenization are an approximation of the equations governing the real phenomena. But, in this context it is obviously that in the future it will be necessary to have also numerical evidences.

Timisoara
December 1998

Stefan Balint

1. On the determination of the radial segregation of dopant in the case of semiconductor crystal growth in Bridgman - Stockbarger configuration

1.1 Introduction

The compositional uniformity of crystals grown from the melt depends strongly on the pattern and intensity of flow in the melt and on the shape of the melt/solid interface. In the processes such as the Czochralski and floating zone methods and the vertical Bridgman-Stockbarger configuration studied here, the unequal partitioning of dopant between melt and crystal during solidification causes a concentration gradient perpendicular to the melt/solid interface. When this interface is planar and the melt is quiescent, except for motion caused by crystal growth, the concentration field decays exponentially with distance into the melt. Curvature of the solidification interface and convection in the melt, both change the concentration distribution along the interface and alter the dopant level in the crystal.

The influence of convection on segregation in the growth direction (axial segregation) was pointed out by the Burton's et al. analysis [1-3] of the effect of crystal rotation on mass transfer. When the crystal diameter is large and the velocity field is similar along the radius of the melt/solid interface, convection only alters the concentration field perpendicular to the interface. Burton et al. analyzed this case and developed an expression for an effective segregation coefficient and introduced the notion of an axial "boundary layer" thickness for diffusion-controlled mass transfer. Others

[4-8] applied the idea of a uniform diffusion-layer or stagnant-film that is masking a growing crystal from a well mixed bulk and have determined so-called boundary-layer (more appropriately diffusion-layer) thickness without any picture for the fluid motion in the melt. Other than Burton, Prim and Slichter's original analysis of rotating flow few papers dealing with melt crystal growth [9,10] have addressed the exact coupling between the fluid flow and mass transfer in a consistent way.

In many growth configurations, the concept of a uniform diffusion-layer yields an over-simplified view of the role of convection in dopant segregation [11]. When the flow is laminar and cellular, as in the case for many small-scale growth systems and for reduced gravity experiments,

convective mass transfer is uneven along the surface of the crystal and significant lateral segregation results. The coupling between moderate convection and lateral dopant segregation thoroughly analyzed for the rotationally-driven flows in small-scale floating zones [10,12,13] and has been demonstrated for buoyancy-drive convection under microgravity conditions [14]. All this studies were of model crystal growth systems with planar solidification interfaces.

Coriell and Sekerka [15] (also see ref. [16]) demonstrated that significant radial segregation occurs in systems without convection tangent to the crystal surface when the radius of curvature of this interface is the same or less than the length scale of the concentration gradient adjacent to the interface. Curvature induced segregation was shown to be an important contribution to dopant inhomogeneity in capillary growth systems [17-19] and may be important in other small-scale crystal growth experiments in which convection in the melt has been suppressed.

We consider the prototype vertical Bridgman - Stockbarger growth system presented in Fig.1.

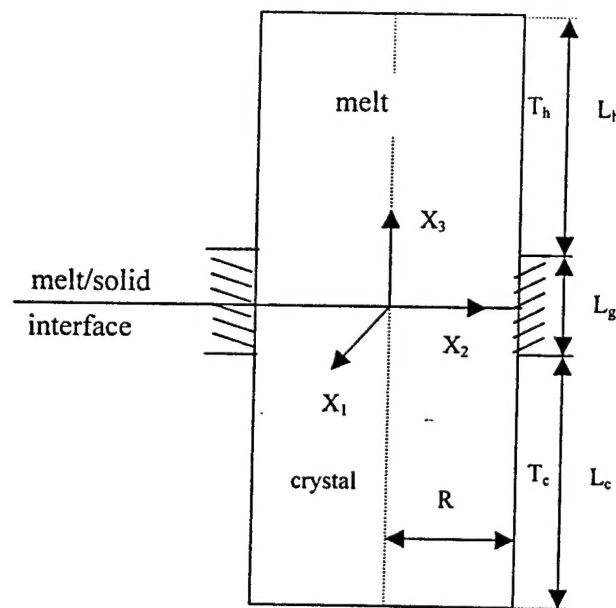


Fig.1. Geometry of the prototype vertical B-S system

The influence of the natural convection governed by the equations

$$\begin{aligned}
(1) \quad & \frac{\partial \bar{v}}{\partial t} + \bar{v} \cdot \nabla \bar{v} = -\nabla p + \text{Pr} \cdot \nabla^2 \bar{v} - \text{Ra} \cdot \text{Pr} \cdot \theta \cdot \bar{e}_3 \\
(2) \quad & \frac{\partial \theta}{\partial t} + \bar{v} \cdot \nabla \theta = \nabla^2 \theta \\
(3) \quad & \nabla \cdot \bar{v} = 0
\end{aligned}$$

on the dopant dispersion governed by the equation

$$(4) \quad \frac{\partial c}{\partial t} + \frac{\text{Sc}}{\text{Pr}} \cdot \bar{v} \cdot \nabla c = \nabla^2 c$$

was analyzed by C.J. Chang and R.A. Brown in [20]. The calculations described here are of the axisymmetric steady state velocity, temperature and concentration fields and melt/solid interface shapes. The mathematical free-boundary problem that describes these variables is solved by finite-element/Newton technique that computes simultaneously the shape of the solidification interface, the velocity and pressure fields in the melt and the temperature distribution in both melt and crystal. Flow field calculated with the finite-element/Newton algorithm are used in a separate calculation of the distribution of a dilute dopant within the melt and crystal. The bulk of the calculations reported here are for a melt and crystal with thermophysical properties similar to those of the gallium-doped germanium system.

Three distinct types of flow patterns were observed. At low Rayleigh numbers ($\text{Ra} < 10^3$) the streamlines were rectilinear and only slightly distorted by buoyancy forces. For intermediate values of Ra ($10^3 \leq \text{Ra} \leq 10^6$) a cellular flow developed which was driven by the radial temperature gradients established by the mismatch in thermal boundary conditions between the adiabatic and hot zones. The flow moved upward along the sidewall and downward at the centerline of the ampoule. The center of the cell was located slightly above the gradient zone and migrated downward and toward the sidewall with increasing Ra . Increasing the Rayleigh number to 2.6×10^6 led to the development of a weak secondary cell adjacent to the melt/solid interface. The outset of the multi-cellular flows marks the start of the third type of flow pattern. The motion in the secondary cell next to the interface was in the opposite direction to the main cell and led to qualitatively different radial segregation than the flows with a single cell which exist for Ra less than 1×10^6 .

The temperature fields show the effect of the Prandtl number in the gallium germanium system. For Rayleigh numbers between zero and 1×10^4 the thermal fields in both the melt and crystal were essentially the same as the field calculated without convection ($Ra=0$) and were similar to results of Fu and Wilcox [21]. Increasing Ra above 1×10^4 caused the isotherms along the axis of the melt to compress toward the melt/solid interface by the downward fluid motion. By $Ra = 5 \times 10^6$ the shape of several isotherms farthest from the interface inverted from convex to concave at the center of the melt. The isotherms in the crystal were unchanged by changing Ra . Also, the fact that a large position of the crystal was at the uniform temperature $\theta=0.1$ demonstrated that the length of ampoule in the cold portion of the furnace was sufficient to guarantee that the position of the end of the ampoule was unimportant.

The shape of the melt/solid interface was unchanged by convection for Ra between 0 and 10^3 . For higher Rayleigh numbers, the hot melt moving down the axis of the ampoule drove the melt/solid interface deeper into the adiabatic region. The changes in interface shape caused by convection were not large; even for $Ra = 5 \times 10^6$ the deflection of the interface was only 6% of its mean location.

Dopant fields were calculated for the velocity field and melt/solid interface shapes discussed above for the segregation coefficient $k=0.1$ and Schmidt number $Sc=10$ similar to the gallium-doped germanium system. The almost parallel iso-concentration lines for Rayleigh numbers up to 10 correspond to the one-dimensional solidification model. The concentration field was deformed at higher values of Ra ; at $Ra = 1 \times 10^4$ the concentration field had the beginnings of the uniform core of melt with steep concentration gradients along each boundary, consistent with the boundary-layer model for a well-mixed melt. A large amount of radial segregation was present even at this level of convection: flow downward along the axis swept dopant from crystal and induced radial segregation across the surface of the crystal. The change in concentration across the interface evolved with increasing Ra from approximately 1% segregation caused by interface curvature at $Ra=0$ to almost 70% of the mean value $1/k$ for the worst case of $Ra = 1 \times 10^3$. The radial variation of dopant decreased with the more intense flow motion that corresponded to $Ra=10^4$. The maximum in radial segregation with increasing convection found here was consistent with calculations of Nikitan for the growth of gallium-doped germanium in a horizontal boat.

The percent radial segregation, defined as $\Delta c = [c(0, h(0)) - c(\Lambda, h(\Lambda))] \times 100/k$ reached a maximum for the flow corresponding to nearly $Ra=10^3$ and

decreased for larger values of Rayleigh number. The value of the segregation coefficient set the mean concentration in the melt at the interface and affected the level of radial segregation in the crystal. The exponentially decreasing concentration profile present at low values of Ra extended further into the melt for smaller segregation coefficients and made the concentration field more sensitive to convection. Consequently the level of segregation Δc was higher for lower k.

Changing the diffusivity of the solute also had a marked effect on the level of radial segregation. At high Schmidt numbers and Rayleigh numbers of 1×10^3 and above, the isoconcentration curves developed fingers oriented parallel to the melt solid interface that corresponded to extremely rapid variation in composition within a distance of the same order of magnitude at the thickness led to large (over 100%) radial segregation.

The complicated segregation patterns discussed created doubts as to the applicability of the simple "diffusion-layer" or stagnant-film model for correlating axial segregation behavior. Details results for the velocities and dopant profile make possible to check this correlation. To do this, radially

averaged concentration profiles, defined as $\bar{c}(z) \equiv \int_0^{\Lambda} c(r, z) \cdot r \, dr$ was

calculated for different values of Ra, k and Sc. For low Rayleigh numbers ($0 \leq Ra \leq 1 \times 10^2$), these radially averaged profiles were essentially the same as the concentration profiles predicted by one-dimensional models which account only for the convection caused by crystal growth. A region of nearly uniform average concentration $\bar{c}(z) = c_B$ developed with increasing Ra. The profile for $Ra = 1 \times 10^4$ was divided into a region of thickness δ_f with steep dopant gradient adjacent to the crystal, a zone of uniform concentration and a gradient zone caused by the fictitious inlet condition at the top. These profiles were reminiscent of the form assumed by a stagnant film model and suggest the equivalence of δ_f with the width of usual diffusion layer. The thickness δ_f were compared with results of this approach through calculation of effective segregation coefficient. The effective segregation coefficient appropriate for a true unsteady Bridgman system with $\Lambda = 0.25$ was approximated as $k_{\text{eff}} = c_s / c_B = 1 / c_B$ where c_s was the dimensionless average concentration across the crystal.

If a diffusion layer of thickness $\delta = \bar{\delta} / L$ existed that separated the crystal surface from bulk melt at concentration c_B , the effective segregation coefficient k_{eff} would be derived following Flemings formula as

$$k_{\text{eff}} = \frac{c_s}{c_B} = \frac{k}{k + (1 - k) \exp(-V_L \cdot \delta / D)} \text{ or in dimension less form used here}$$

$$\text{as } k_{\text{eff}} = \frac{k}{k + (1 - k) \exp(-\sigma \cdot \delta \cdot \text{Pe} \cdot \text{Sc} / \text{Pr})}.$$

Rearranging this yielded an explicit relation for the diffusion-layer thickness

$$\delta = -\frac{\text{Pr}}{\text{Pe} \cdot \text{Sc} \cdot \sigma} \cdot \ln \left(\frac{k}{k_{\text{eff}}} \cdot \frac{1 - k_{\text{eff}}}{1 - k} \right). \text{ Values of } \delta \text{ computed from the above}$$

formula with k_{eff} calculated from the finite-element results are compared to values of δ_f measured from the profiles of $\bar{c}(z)$. In each case, δ and δ_f were of the same order of magnitude but different by as much as a factor of two. This result is not surprising. Within the distance δ_f from the crystal in the finite element calculation, the velocity field was a combination of the growth velocity and a contribution from natural convection. These two components were of the same order of magnitude and it was the latter component which caused the discrepancy between δ and δ_f which led to radial segregation.

One of the main conclusions of Chang and Brown in the paper [20] concerning the steady state is the following:

“For moderate levels of convection the “stagnant film” or “diffusion-layer” model is a gross oversimplification of the interaction between complicated flow patterns and the dopant field. Diffusion-layer thicknesses δ determined by the formula

$$(5) \quad \delta = \frac{\text{Pr}}{\text{Pe} \cdot \text{Sc} \cdot \sigma} \cdot \ln \left(\frac{k}{k_{\text{eff}}} \cdot \frac{1 - k_{\text{eff}}}{1 - k} \right)$$

and experimental data are, at the best, empirical fits to effective segregation coefficient, for the crystal/melt system. The comparison demonstrates that, although the radial averaged diffusion-layer thickness determined from the finite-element simulations and formula (5) are of the same order of magnitude, the actual concentration gradient adjacent to the crystal is far from radial uniform. As much 60% radial segregation can exist. Only detailed calculations of the exact interaction of fluid flow and dopant profile adjacent to the interface can be used to estimate the level of radial segregation in crystal. Our study of a prototype Bridgman system gives qualitative understanding of fluid flow and dopant segregation in actual growth system and will serve as the starting point for more refined calculations, aimed at comparison with experiment in well-characterized small-scale system”.

Starting from this, we propose a new model in which the "precristallization zone" or "mushy zone" substitutes the "stagnant film" or "diffusion-layer" like M.B. Tahar in [22]. Tahar approach this solid-liquid mushy zone using a model of a porous media with evolving heterogeneity, and adapt a spatial averaging method to derive macroscopic equations describing geometry of the dendritic structure as well as dispersive effects. For as the "mushy zone" is a thin bed of periodically distributed solid inclusions, which are small with respect to the distance between two neighboring inclusions (we shall say that the concentration is small).

The diffusion-layer thicknesses δ are substituted by the "mushy zone" thicknesses which can be determined by X-ray diffraction measurements. In this way the diffusion-layer or stagnant film masking the growing crystal is substituted by a thin periodic porous medium bounded below by an impermeable rigid wall which is the melt/solid interface.

If the size of solid inclusions is smaller like the critical size (see [23]) the flow in "mushy-zone" is the global flow given by (1)-(3).

If the size of solid inclusions is critical (see [23]) the flow in the mushy zone is a Brinkman flow, determined by the global pressure and respecting at the "mushy-zone" and "pure-fluid" interface the Beavers-Joseph or Jones modified Beavers-Joseph or Rudriah conditions (see [24],[25],[26]).

If the size of solid inclusions is larger like the critical size (see [23]) then the flow in the "mushy-zone" is a Darcy flow, determined by the global pressure and respecting at the "mushy-zone" and "pure-fluid" interface Rudriah conditions (see [26]).

The dispersion mechanism of the dopant in mushy-zone is due to the diffusion and convection, which exists simultaneously, and is assumed that balance each other or convection dominates diffusion. Obviously the mechanism takes into account also the existence of some solid inclusions. This dispersion mechanism model for the dopant adjacent to the interface is more refined as the dispersion mechanism in diffusion-layer model as well as the dispersion mechanism described by equation (4) and is governed by a new convective-diffusive equation which generalize equation (4).

In the new convective-diffusive equation we use the velocity field the melt/solid interface defined by (1)-(3) and a certain periodic microstructure similar with the microstructure of the crystal.

We find also the stationary solutions without radial segregation of the new convective-diffusive equation and perturbations with respect to these solutions are asymptotically stables. We establish also the optimal control for the stationary solutions without radial segregation.

1.2 The flow in the mushy zone

For a periodic material $\Omega \subset \mathbb{R}^3$ for which the period is a cubic cell homotetic with a small ratio ε of the unit cell $Y = [-1/2, 1/2]^3 \subset \mathbb{R}^3$, in which the fluid domain Y_F and the solid on Y_S have a smooth boundary Γ (like in Fig.2.), using homogenization method it was deduced a macroscopic model, from microscopic processes, assuming that the flow is slow and the size of the solid inclusions is of the same order like the size of the cell (low porosities) (see [27], [28], [29]).

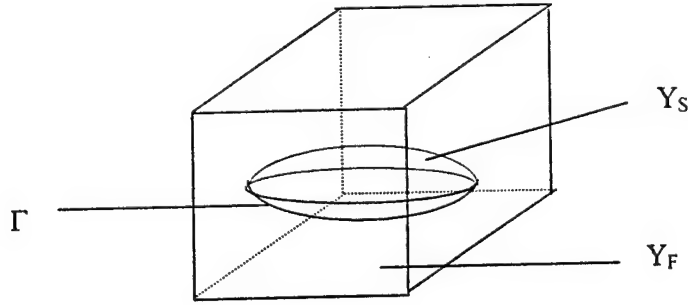


Fig.2. The unit cell Y

In the macroscopic model the flow $\langle \bar{v} \rangle(x)$ is given by Darcy's law

$$(6) \quad \langle \bar{v} \rangle(x) = -K \cdot \nabla_x p^0, \quad x \in \Omega$$

where K is the permeability tensor defined by the coefficients K_{ij} given by

$$(7) \quad K_{ij} = \frac{1}{|Y|} \int_{Y_F} v_i^j dy$$

and v_i^j are the components of the micro velocity fields defined in the unit cell Y by the following boundary value problem.

$$(8) \begin{cases} \mu \Delta_y \bar{v}^j = \nabla_y q^j - \bar{e}_j & \text{in } Y_F \\ \nabla_y \bar{v}^j = 0 & \text{in } Y_F \\ \bar{v}^j = 0 & \text{on } \Gamma \quad j=1,2,3 \\ \bar{v}^j \text{ and } q^j \text{ are } Y \text{ periodic} \\ \bar{e}_j \text{ is the unit vector in } y_j \text{ direction} \end{cases}$$

In formula (6) $\nabla_x p^0$ represents the pressure gradient in Ω . Numerical calculus of the permeability tensor coefficients K_{ij} , solving (8) by finite-elements method, was performed by Chiang. C. Mei, Jean-Luis Auriault and Chiou-On Ng in the paper [30] and by Cheo K. Lee, Chin-Cheng Sun and Chiang C. Mei in [31]. They consider the case when the solid inclusion is a Wigner-Seitz grain in the unit cell Y . In this case due to the symmetry, $K_{ij} = 0$ for $i \neq j$ and $K_{11} = K_{22} = K_{33}$. Therefore it is sufficient to consider only K_{11} induced by the unit pressure gradient in \bar{e}_1 direction. Computation

have been performed for porosities $\pi_Y = \frac{|Y_F|}{|Y|} = 1 - \frac{|Y_S|}{|Y|}$ in the range

$0.2518 < \pi_Y < 0.8333$ and the results were compared to the values of the permeability given by the well known empirical Kozeny-Carman formula

$$(9) \quad k = \frac{1}{5} \cdot \frac{\pi_Y^3}{(1 - \pi_Y)^2} \cdot \left(\frac{V_s}{A_s \cdot \ell} \right)^2$$

where V_s is the volume, A_s is the area of the grain, and ℓ is one side of the cube.

Within the range $0.37 < \pi_Y < 0.68$ for which the empirical formula is based on experiments, the results are consistent and in trend with, but fall slightly below the empirical formula. Outside this range of porosities, the deviation increases.

It should be noted that, the Kozeny-Carman formula is the best fit to experimental data for all grain shapes, but outside of the range of porosities $0.37 < \pi_Y < 0.68$ is an extrapolation of measured data and may not be totally accurate.

In the paper [31] results were compared to numerical values obtained by Zick and Homsey in [32] for uniform spheres of various packings.

Discrepancies between the packed spheres and Wigner-Seitz grains appear for close packing (low porosity), since particle interaction is affected by the geometry most significantly. At higher porosity, the results agree remarkably well.

Other results concerning the permeability tensor coefficients in the case of dendritic growth are given in [22] and in general in the case of solidifications in [33-45].

In the paper [23] Th. L  vy studies slow flow of an incompressible viscous fluid in an array of a great number of small fixed particles assuming that the particle size ϵ and the distance η between two neighboring solids (η is also the size of the period) are such that $\epsilon \ll \eta \ll 1$. This assumption corresponds to low concentration of solid inclusions (high porosity). She proves that there exists a critical size for particles, for which Brinkman's flow occurs. For smaller sizes solid do not influence the flow and for larger particle sizes the fluid flow is governed by Darcy's law.

In this case it is worthwhile obtaining approximate homogenization formulas simpler than the usual ones. This way be done by disregarding the interaction between inclusions: the local solutions appearing in the homogenization formulas (which are periodic, the periodicity taking into account the interaction) become solutions in the whole R^3 space (without interaction). In this connection, Einstein in 1906 gave a celebrated formula for the homogenized viscosity of a dilute suspension of rigid solid spherical particles in a viscous fluid. As the general case of non-small concentration involves new phenomena such as variable microstructure, anisotropy and modification of the inertial terms, it is worthwhile obtaining the Einstein's approximation as the asymptotic behavior for small concentration of the homogenization formulas (see [46], [47]).

Returning to the mushy zone where we have supposed that the solid inclusions are small with respect to the distance between two neighboring inclusions according to L  vy's paper if the size of the solid particles is smaller than the critical size then the particles do not influence the global flow, and therefore in mushy zone the flow is the global flow defined by the equations

$$(10) \quad \bar{v} \cdot \nabla \bar{v} = -\nabla p^0 + \text{Pr} \nabla^2 \bar{v} - \text{Ra} \cdot \text{Pr} \cdot \theta \cdot \bar{e}_3$$

$$(11) \quad \bar{v} \cdot \nabla \theta = \nabla^2 \theta$$

$$(12) \quad \nabla \bar{v} = 0$$

where $\nabla = \bar{e}_r \cdot \frac{\partial}{\partial r} + \bar{e}_3 \cdot \frac{\partial}{\partial x_3}$ is the gradient operator in cylindrical coordinates. The Prandtl number Pr and the Rayleigh number Ra appearing in equation (10) and (11) are defined by

$$Pr = \frac{\mu}{\alpha_L}, Ra = \beta \cdot g(T_h - T_c) \cdot \frac{L^3}{\alpha_L} \cdot \mu.$$

This case corresponds to the case considered in [20] and other papers. If the size of the solid inclusions is critical then the flow in the mushy zone is a Brinkman flow governed by a Brinkman's law

$$(13) \quad \mu \Delta \langle \bar{v} \rangle = \nabla p^0 + \mu \cdot \varphi \cdot H \cdot \langle \bar{v} \rangle$$

where φ is the volume concentration of solid particles and H is the translation tensor.

If the size of solid particles is greater than the critical size then the flow is a Darcy flow governed by a Darcy's law

$$(14) \quad \mu \cdot \varphi \cdot H \cdot \langle \bar{v} \rangle = -\nabla p^0$$

The permeability tensor K , that appears in critical and supercritical case, is expressed in terms of the particles concentrations φ and the translation tensor H : $K = \frac{1}{\mu \varphi} \cdot H^{-1}$.

In subcritical case is not necessary to put coupling conditions but in supercritical case is absolutely necessary to put this kind of conditions in order to realize the continuity of the velocity field. In this order we will use Beavers-Joseph postulate according to which the slip velocity at the permeable interface differs from the mean filtration velocity within the porous matrix, and the shear effects are transmitted into the body of the material through a boundary-layer region. Across this boundary the velocity changes rapidly from this value at the interface to the Darcy's law value given by

$$(15) \quad u_m = -\frac{K'}{\mu} \cdot \frac{dp}{dx}$$

in porous medium (like in Fig.3.).

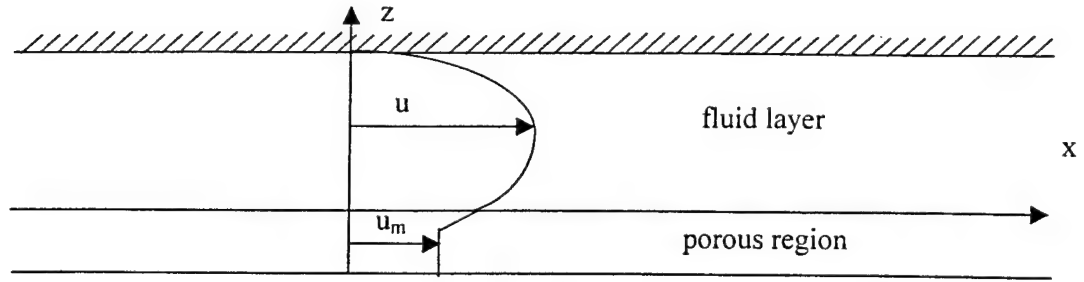


Fig.3. Physical model for Beavers-Joseph slip condition

Beavers and Joseph also assumed that the slip velocity for the free fluid is proportional to the shear rate at the permeable boundary and is related to the slip velocity of the exterior flow by an adhoc boundary condition

$$(16) \quad \left. \frac{du}{dz} \right|_{z=0_+} = \Phi \cdot (u - u_m)$$

where 0_+ is the boundary limit point from the exterior fluid, and Φ is a constant which depends on the properties of the fluid and the porous matrix, but is independent of spatial coordinates. They showed that $\Phi = \alpha / \sqrt{K'}$

where α is a dimensionless quantity depending on the material parameters which characterizes the structure of the permeable material within the boundary region. Therefore the Beavers-Joseph slip condition at the interface can be written as:

$$(17) \quad \frac{du}{dz} = \frac{\alpha}{\sqrt{K'}} (u - u_m)$$

where u and du/dz are evaluated at the interface 0_+ , while u_m is evaluated at some small distance d given by

$$(18) \quad d = \frac{\sqrt{K'}}{\alpha}$$

away from the plane $z = 0$ in porous side. Since the parameter α is obtained from a dimensional analysis and is not defined mathematically it needs to be evaluated from the experimental data. Beavers and Joseph conducted experiments to determine the validity of the above model and reported α for three kinds of foametal and two kinds of aloxite matrices ($6.5 \times 10^{-10} < K' < 8.2 \times 10^{-8} \text{ m}^2$). Their data also demonstrated that α is almost independent of the fluid viscosity μ (see [48]). Although the Beavers-Joseph condition was

first presented as an empirical result, a certain amount of theoretical foundations was later provided and several experimental investigations supported it. In any case Beavers-Joseph condition permits to find the small distance d where we make the coupling between the slip velocity and the mean filtration velocity with formula:

$$(18') \quad u_c = \frac{\alpha}{\sqrt{K'}} (u - u_m) \cdot z + u \quad \text{for } -d \leq z \leq 0.$$

In the paper [12] Jones argued that the Beavers-Joseph condition was essentially a relationship involving shear stresses rather than just the velocity shear, and suggested a generalized form (17) as

$$(19) \quad \frac{\partial u}{\partial z} + \frac{\partial w}{\partial x} = \frac{\alpha}{\sqrt{K'}} (u - u_m) \quad \text{Jones - modified Beavers - Joseph condition}$$

where $\bar{v} = (u, v, w)$.

It is understood that $u, \frac{\partial u}{\partial z}, \frac{\partial w}{\partial x}$ are evaluated at the interface $z = 0_+$, while u_m is evaluated at some small distance d given by

$$(20) \quad d = \left(\frac{\alpha}{\sqrt{K'}} - \frac{\partial w / \partial x}{u - u_m} \right)^{-1}.$$

Taylor in [49] observed that the Beavers-Joseph condition can be deduced if the Brinkman flow model is used in a region very close to the fluid-porous layer interface while the flow in the bulk of the porous medium is governed by Darcy law. The idea was extended by Neale and Nader in [50] who showed that for the problem of flow in a channel bounded by a thick porous wall, the Brinkman equation yields the same solution of that obtained from the Darcy equation provided α is taken as $(\mu' / \mu)^{1/2}$, where μ' is the effective viscosity for the fluid/saturated porous medium.

Ross in [51] developed an equation for the average fluid velocities in terms of gradients of average pressure and velocities and, indirectly, the geometry of the porous interface by considering the flow of inertial fluid through the pores. Using an averaging procedure, he obtained the interfacial slip condition for the Beavers-Joseph flow problem as:

$$(21) \quad u = -\frac{K'}{\mu} \cdot \frac{dp}{dx} + K' \cdot L_z \cdot \frac{du}{dz} + K' \cdot N \cdot \frac{d^2 u}{dz^2}.$$

The term of the left hand side and the first two terms on the right-hand side of this equation are identical to that in equation (17) except that the first term (equation (21)) represents the Darcy flow at the interface $z=0$ and not at $z<0$

as in the Beavers-Joseph model. Therefore neglecting the second order viscous term in (21) and considering the Darcy's flow at $z < 0$ we obtain the Beavers-Joseph model with $\alpha = \sqrt{K'}/L_z$. Ross employed a scale analysis, to show that all the three terms in equation (21) are of equal order-of-magnitude, and the second order viscous term must be retained for the slip condition to be valid. A generalized slip condition for an anisotropic porous medium was presented as:

$$(22) \quad u_i = -\frac{K'_{ij}}{\mu} \cdot \frac{\partial p}{\partial x_j} + K'_{ij} \cdot L_{j p q} \cdot \frac{\partial u_p}{\partial x_q} + K'_{ij} \cdot N_{j p} \cdot \nabla^2 u_p,$$

where $K'_{ij} = \mu \cdot K_{ij}$ and K_{ij} is the permeability tensor and $L_{j p q}$, $N_{j p}$ are expressed in terms of line and area integrals.

Note that in the above results, the porous medium is dense and of large thickness as compared to the interface boundary layer.

Rudraiah in [26] examines the effect of porous layer thickness on slip velocity at the interface, particularly when the porosity is large. Modified Beavers-Joseph expressions were obtained for two cases: a) porous layer bounded below by a thick layer of static fluid, and b) porous layer bounded below by an impermeable rigid wall. For case b) the slip condition was found as:

$$(23) \quad \frac{du}{dz} = \left(\frac{\lambda'}{K} \right)^{1/2} \cdot \left[\frac{\varepsilon \cdot \lambda' \cdot u_m}{\sinh(\delta \cdot h')} + (u - u_m) \cdot \coth(\delta h') \right]$$

where h' is the thickness of the porous layer, $\delta = (\lambda' \cdot K)^{-1/2}$, and λ' is a viscosity parameter. Equation (23) reduces to the Beavers-Joseph condition as $h' \rightarrow +\infty$ and a comparison with equation (17) shows that $\lambda' = \alpha^2$, which agrees with the finding of Weale and Nader in [50] if λ' can be identified as the viscosity ratio μ'/μ . It is understood that in equation (21), u , du/dz are evaluated at the interface $z = 0_+$ while u_m is evaluated at some small distance d given by

$$(24) \quad d = \frac{\sqrt{K}}{\alpha} \left[\coth(\delta \cdot h') + \frac{\varepsilon \cdot \alpha^2 \cdot u_m}{\sinh(\delta \cdot h')} \cdot \frac{1}{u - u_m} \right]^{-1}$$

Returning to the mushy zone, this is located in the region $\Omega = \{(x_1, x_2, x_3) \in \mathbb{R}^3 \mid 0 \leq x_1^2 + x_2^2 < R^2, 0 < x_3 < h'\}$ and the fluid layer in the region $\Omega' = \{(x_1, x_2, x_3) \in \mathbb{R}^3 \mid 0 \leq x_1^2 + x_2^2 < R^2, h' < x_3 < L_h\}$. The permeable interface is located on the level $x_3 = h'$. Due to the small thickness and large porosity of the mushy zone we will use Rudraiah slip condition for assuring the continuity of the velocity field.

Once global velocity field \bar{v} and pressure field p^0 in the melt are determined from the two phase natural convection problem described by equations (10), (11), (12) in super critical case we use the pressure field p^0 in order to find, with formula (14), the Darcy's flow $\langle \bar{v} \rangle$. With this flow $\langle \bar{v} \rangle$ and the global velocity field \bar{v} using (22) we find the small distance d where we make the coupling between the global flow \bar{v} and Darcy's flow $\langle \bar{v} \rangle$. Therefore we will have the Darcy flow just in the region $0 \leq x_3 \leq d < h'$.

1.3 The transport equation of the dopant in mushy zone when convection and diffusion balance each other

Using homogenization method in the case when convection and diffusion balance each other (at the global level) we can obtain (see [52]) the following transport equation for a solute in a periodic porous media:

$$(25) \quad \frac{\partial c}{\partial t} + \frac{1}{\pi_Y} \cdot \sum_{i=1}^3 \langle v_i \rangle \cdot \frac{\partial c}{\partial x_i} = \sum_{i=1}^3 \sum_{j=1}^3 D_{ij} \cdot \frac{\partial^2 c}{\partial x_i \partial x_j}$$

In this equation $c = c(t, x)$ is the solute concentration, $\langle v_i \rangle = \langle v_i \rangle(x_1, x_2, x_3)$, $i = 1, 2, 3$ are the components of the fluid velocity given by Darcy's law and the coefficients D_{ij} are the components of the diffusion (dispersion) tensor. These components are given by the formula

$$(26) \quad D_{ij} = D \left(\delta_{ij} + \frac{1}{|Y|} \int_{Y_F} \frac{\partial \chi_i}{\partial y_j} dy \right) = D \left(\delta_{ij} + \frac{1}{|Y|} \int_{\Gamma} \chi_i \cdot n_j d\sigma \right)$$

In the above formulas D is the diffusion (dispersion) coefficient of the solute and χ_i is the solution of the following boundary value problem

$$(27) \quad \begin{cases} \Delta_y \chi_i = 0 & \text{in } Y_F \\ \bar{n} \cdot \nabla_y \chi_i = -n_i & \text{on } \Gamma \\ \chi_i & \text{is } Y \text{ periodic} \\ \langle \chi_i \rangle = \frac{1}{|Y|} \int_{Y_F} \chi_i dy = 0 \end{cases}$$

for $i = 1, 2, 3$.

Multiplying equation $\Delta_y \chi_i = 0$ by χ_j and integrating on Y_F we obtain for the components D_{ij} the following formula

$$(28) \quad D_{ij} = D \left[\delta_{ij} - \frac{1}{|Y|} \int_Y \nabla \chi_i \cdot \nabla \chi_j dy \right]$$

and consequently D_{ij} is symmetric ($D_{ij} = D_{ji}$).

In addition we have

$$(29) \quad D_{ij} = D \cdot \langle \nabla B_i, \nabla B_j \rangle = D \cdot \frac{1}{|Y|} \int_{Y_F} \sum_{k=1}^3 \frac{\partial B_i}{\partial y_k} \cdot \frac{\partial B_j}{\partial y_k} dy$$

where $B_i = -\chi_i - y_i$ and consequently the tensor D_{ij} is positive.

If Y_S is symmetric to any coordinate planes then $D_{ij} = 0$ for $i \neq j$ and consequently the dispersion tensor is diagonal.

When the solid inclusions are small with respect to the distance between two neighbouring inclusions using results from [46] and [47] in [53] was proved that for symmetric solid inclusions we have

$$(30) \quad D_{ij} = D \left(1 - \varphi + \frac{\varphi}{|Y_S|} \int_{\Gamma} \chi_i n_i d\sigma \right) \delta_{ij}$$

where φ is the volume concentration of solid inclusions and is assumed to be small. The functions χ_i are solutions of the external Neumann problem:

$$(31) \quad \Delta \chi_i = 0 \quad \text{in } \mathbb{R}^3 \setminus Y_S$$

$$(32) \quad \Delta \chi_i \cdot \bar{n} = -n_i \quad \text{on } \Gamma$$

In [54] we have find the transversal ($D_{11}=D_{22}$) and longitudinal (D_{33}) diffusion coefficients for the prolate spheroids. They are plotted as function of the excentricity on the following figures.

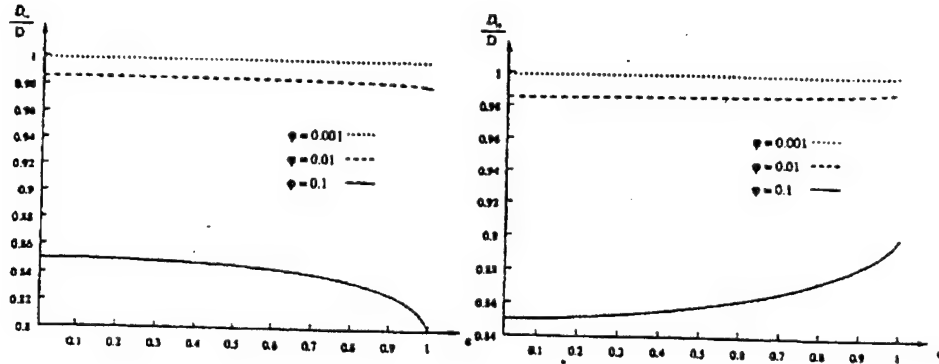


Fig.4.

Therefore the dopant transport in mushy zone is given by (25) where D_{ij} are given by (30) and $\langle v_i \rangle$ are the component of the velocity field of the global convection flow, Brinkman's flow or Darcy flow.

Steady state solutions of equation (25) are given by equation

$$(33) \quad \frac{1}{\pi_Y} \sum_{i=1}^3 \langle v_i \rangle \cdot \frac{\partial c}{\partial x_i} = \sum_{i=1}^3 \sum_{j=1}^3 D_{ij} \frac{\partial^2 c}{\partial x_i \partial x_j}$$

This equation generalizes the steady state mass balance equation

$$(34) \quad \frac{Sc}{Pr} (\bar{v} \cdot \nabla \tilde{c}) = \nabla^2 \tilde{c}$$

used in [20] for the determination of the dopant field in the melt. In equation (34) the Schmidt number $Sc = \mu/\mathcal{D}$ and the Prandtl number $Pr = \mu/\alpha_L$. \mathcal{D} is the diffusivity of Ga in Ge, α_L is the thermal diffusivity in liquid. Boundary conditions used in [20] for solving (34) are

$$(35) \quad \bar{N} \cdot \nabla \tilde{c} = \frac{Pe \cdot Sc}{Pr} (\bar{e}_z \cdot \bar{N}) \cdot (1-k) \tilde{c}; \quad 0 \leq r \leq \Lambda, \quad z = h(r)$$

$$(36) \quad \frac{\partial \tilde{c}}{\partial z} = \frac{Pe \cdot Sc}{Pr} (\tilde{c} - 1) \quad 0 \leq r \leq \Lambda, \quad z = 0$$

$$(37) \quad \frac{\partial \tilde{c}}{\partial r} = 0; \quad r = 0, \Lambda, \quad 0 \leq z \leq 1$$

where $z = h(r)$ represents the location of the melt/solid interface, $\Lambda = R/L$, R is the radius and L is the length of ampule, \bar{N} is the unit vector normal to the interface, $Pe = V_S \cdot L / \alpha_L$ is the Péclet number, k is the segregation coefficient of Ga in Ge.

Equations (35), (36) express conservation of mass at the melt/solid interface, and the fictitious "inlet" at the melt end ($z = 0$) of the ampule respectively. Equation (37) is the no flux condition valid at the centerline and sidewalls of the ampule.

Once the velocity field in the melt and the shape of melt/solid interface were determined from the two phase natural convection problem: equations (34) - (37) are reduced to a linear set to be solved for concentration distribution through the melt.

Returning to equation (33) boundary conditions for solving this equation can be formulated starting from the location of the mushy zone.

We have already supposed that the mushy zone is located in the region

$$(38) \quad \Omega = \left\{ (x_1, x_2, x_3) \mid x_1^2 + x_2^2 < R^2 \text{ and } 0 < x_3 < h' \right\}$$

and from (35) it follows that we have equation

$$(39) \quad \frac{\partial c}{\partial x_3} = - \frac{Pe \cdot Sc}{Pr} (1 - k) c, \quad 0 \leq r \leq R, \quad x_3 = 0$$

which expresses conservation of mass at the melt/solid interface.

From equation (37) which expresses the no flux condition at the centralline and sidewalls it follows

$$(40) \quad \frac{\partial c}{\partial r} = 0, \quad r = 0, R; \quad 0 \leq x_3 \leq d$$

Equation (36) must be substituted by a coupling condition at the level $x_3 = d$ between the concentration field \tilde{c} defined by (34) - (37) and the concentration field c which satisfies (33), (39) and (40) for $x_3 < d$. We can realize this coupling putting

$$(41) \quad c(x_1, x_2, d) = \tilde{c}(x_1, x_2, d)$$

Once the velocity field in "mushy zone" are determined (from equations (10) - (12) or from (13) or from (14)) and \tilde{c} determined from (34) - (37) we can solve (33), (39), (40), (41) and we have the concentration distribution in mushy zone. This dopant field adjacent to the melt/solid interface is a new more refined approach of the real dopant field in this region.

1.4 The transport equation of the dopant in mushy zone when convection dominates diffusion

Using homogenization method, in the case when convection dominates diffusion at global level, we can obtain (see [30]), [31] and [55]) the following transport equation for a solute in a periodic porous media Ω .

$$(42) \quad \frac{\partial c}{\partial t} + \frac{1}{\pi_Y} \sum_{i=1}^3 \langle v_i \rangle \frac{\partial c}{\partial x_i} = \sum_{i=1}^3 \frac{\partial}{\partial x_i} \left(\sum_{j=1}^3 D_{ij} \cdot \frac{\partial c}{\partial x_j} \right)$$

In the above equation $c = c(t, x)$ is the solute concentration, $\langle v_i \rangle = \langle v_i \rangle(x_1, x_2, x_3)$, $i = 1, 2, 3$ are the components of the velocity field and the coefficients D_{ij} are the components of the diffusion (dispersion) tensor. These components are given by the formula

$$(43) \quad D_{ij} = D \left[\delta_{ij} + \frac{1}{|Y|} \int_{Y_F} \frac{\partial \chi_i}{\partial y_j} dy - \frac{1}{|Y|} \int_{Y_F} v_i \chi_j dy \right]$$

In the above formula D is the diffusion coefficient of the solute and $\chi_i = \chi_i(x, y)$ is the solution of the following boundary value cell problem

$$(44) \quad \begin{cases} \Delta_y \chi_i - \bar{v} \cdot \nabla_y \chi_i = v_i - \langle v_i \rangle & \text{in } Y_F \\ \bar{n} \cdot \nabla_y \chi_i = -n_i & \text{on } \Gamma \\ \chi_i \text{ is } Y \text{ periodic} \\ \langle \chi_i \rangle = \frac{1}{|Y|} \int_{Y_F} \chi_i dy = 0 \end{cases}$$

\bar{v} is the velocity field defined by

$$(45) \quad \bar{v}(x, y) = - \sum_{j=1}^3 \frac{\partial p^0}{\partial x_j} \cdot \bar{v}^j$$

where \bar{v}^j are defined by (8), p^0 is the pressure field in Ω and $\langle v_i \rangle = \langle v_i \rangle(x)$ is given by

$$(46) \quad \langle v_i \rangle(x) = \frac{1}{|Y|} \int_{Y_F} v_i(x, y) dy.$$

For a constant gradient pressure field D_{ij} are constants and due to the identity

$$(47) \quad \sum_{i=1}^3 \sum_{j=1}^3 D_{ij} \cdot \frac{\partial^2 c}{\partial x_i \cdot \partial x_j} = \sum_{i=1}^3 \sum_{j=1}^3 \frac{1}{2} (D_{ij} + D_{ji}) \cdot \frac{\partial^2 c}{\partial x_i \cdot \partial x_j}$$

in equation (42) we can use only the symmetric part $D_{ij}^s = \frac{1}{2}(D_{ij} + D_{ji})$ of the diffusion (dispersion) tensor. This symmetric part is given by one of the following three equivalent formulas:

$$(48) \quad D_{ij}^s = D \left[\delta_{ij} + \frac{1}{2|Y|} \int_{Y_F} \left(\frac{\partial \chi_i}{\partial y_j} + \frac{\partial \chi_j}{\partial y_i} \right) dy - \frac{1}{2|Y|} \int_{Y_F} (\chi_i v_j + \chi_j v_i) dy \right]$$

$$(49) \quad D_{ij}^s = D \left[\delta_{ij} + \frac{1}{2|Y|} \int_{\Gamma} (\chi_i n_j + \chi_j n_i) dy - \frac{1}{2|Y|} \int_{Y_F} (\chi_i v_j + \chi_j v_i) dy \right]$$

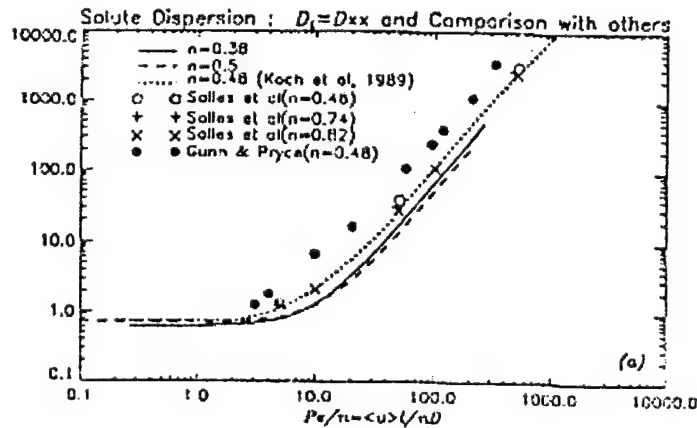
$$(50) \quad D_{ij}^s = D \cdot \frac{1}{|Y|} \int_{Y_F} \sum_{k=1}^3 \frac{\partial B_i}{\partial y_k} \cdot \frac{\partial B_j}{\partial y_k} dy$$

where B_i is defined by

$$(51) \quad B_i = -\chi_i - y_i.$$

If the mean flow is directed along the x_3 axis then D_{ij} is diagonal with two independent components that are the longitudinal D_L and transverse dispersivities D_T ; $D_L = D_{33}$ and $D_T = D_{11} = D_{22}$ (see [17], [18] and [26]). For any other flow direction in the plane Oy_1y_2 , there are four nonzero independent dispersivity coefficients D_{11} , D_{22} , D_{33} and $D_{12} = D_{21}$; $D_{13} = D_{31} = D_{23} = D_{32} = 0$ (see [17], [18] and [26]).

To calculate the dispersion tensor, one must solve the canonical cell problem defined by (44). Lee Sun and Mei in [18] have shown that the cell boundary value problem for convective diffusion of heat can be recast as a variational principle, the case for solute transport being a special case. Computed values of longitudinal and transverse dispersivity coefficients D_L and D_T , for a cubic array of Wigner-Seitz grains, for Péclet number up to 300 for D_L and 200 for D_T , and for two porosities $\pi_Y = 0.38$ and 0.5 are shown in the following figures.



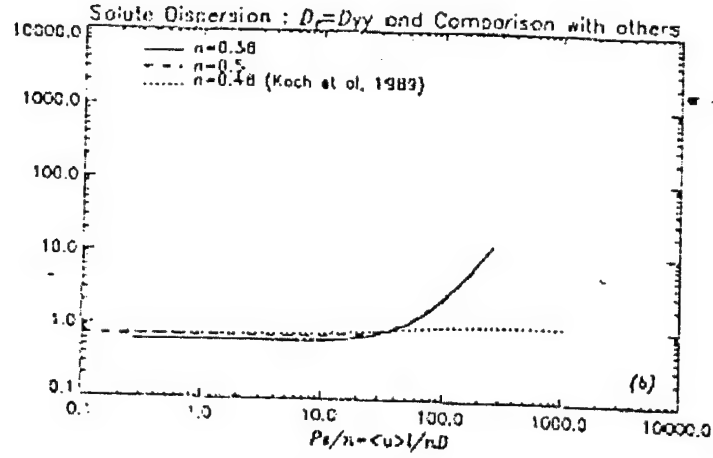


Fig. 5. The solute dispersion coefficients for the Wigner-Seitz grain and comparison with others; (a) the longitudinal dispersion coefficient D_L and (b) the transverse dispersion coefficient D_T .

To conform with experimental literature the abscissas are the Péclet numbers defined in terms of the mean flow velocity averaged over Y_F only, i.e. $\langle v_1 \rangle \cdot \lambda / \pi_Y \cdot D = Pe / \pi_Y$. In Fig. 5(a), the longitudinal dispersivity is also compared with the measured data [57] for simple cubic packing of uniform spheres and the calculations [58] for a simple cubic lattice of uniform spheres with $\pi_Y = 0.48, 0.74$ and 0.82 . The results for $\pi_Y = 0.48$ by Koch et al. [59] based on an approximate analysis for dilute concentrations are also included. All are in qualitative agreement for D_L . From the numerical results for $n = 0.38$ and 0.5 we see that for small Péclet numbers where molecular diffusion is dominant in microcell, the diffusivity is greater for the larger porosity. The reason is that the cross-sectional area through which a passive solute can diffuse increases with porosity. It is always less than unity in the diffusion-dominated regime (at microlevel) since the presence of solid grains reduces the diffusive flux of solute. For large Pe numerical results concerning D_L for Wigner-Seitz cell as well as those by Salles et al. for uniform spheres, are consistent with the experimental measurements [58] and the analytical theory for dilute spheres [59], all showing that D_L increases with $(Pe)^2$, when the mean flow is parallel to a lattice axis. Recall from [59] that if the flow is inclined to a lattice axis, D_L may vary linearly with Pe . In contrast to the case of small Pe , the dependence on porosity is now reversed, and the dispersivity increases with decreasing porosity. Heuristically this is because the velocity gradient in the pores increases as porosity decreases and therefore enhances microscale mixing.

The transverse dispersivity D_T computed for Wigner-Seitz grains is plotted in Fig. 5(b) for $Pe \leq 300$. The qualitative trend is the same as D_L except that

it is less than D_L by roughly two orders of magnitude. Mauri [60] also finds analytically for a dilute lattice of uniform spheres that D_T is proportional to $(Pe)^2$, for small Pe and is eight times smaller than D_L . In contrast Koch et al. in [59] predict that D_T remains almost constant in Pe for very large Pe . There are no reliable measurements for D_T for a regular array of spheres. Some experimental data on D_T for natural granular media are shown in the following figures (see paper [61] - [65]). Although scattered, each individual data set exhibits linear dependence on Pe as D_L .

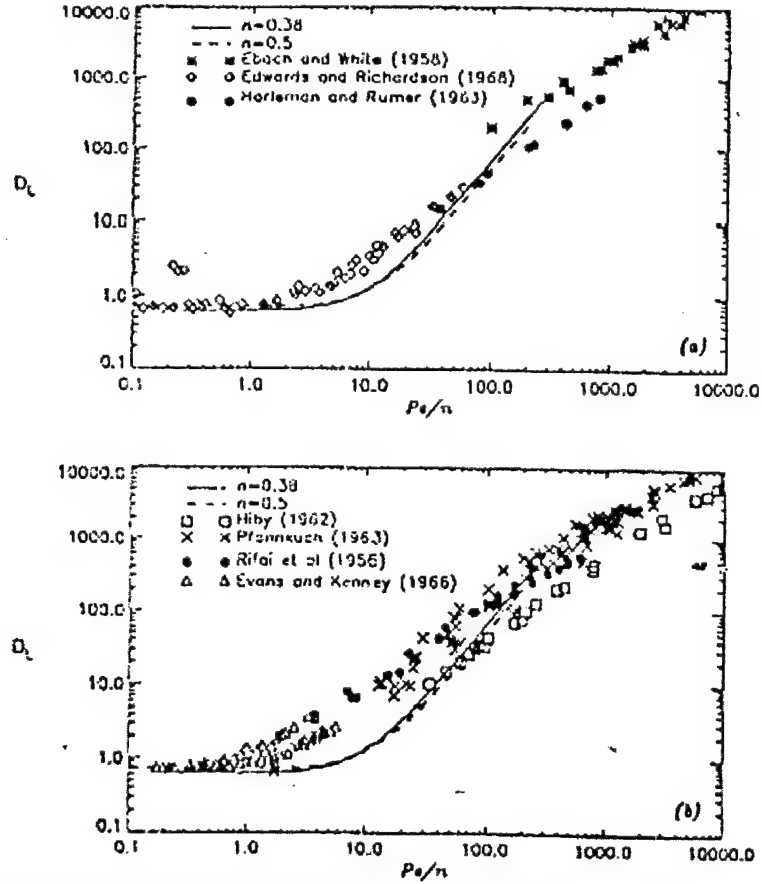


Fig 6 Comparison of D_L for the Wigner-Seitz grain with experimental data for natural granular media.

Steady state solutions of equation (42) for a constant gradient pressure field are given by

$$(52) \quad \frac{1}{\pi_Y} \sum_{i=1}^3 \langle v_i \rangle \cdot \frac{\partial c}{\partial x_i} = \sum_{i=1}^3 \sum_{j=1}^3 D_{ij}^s \frac{\partial^2 c}{\partial x_i \partial x_j}$$

where D_{ij}^s is given by one of the three equivalent formulas (48), (49), (50) and $\langle v_i \rangle$ are the components of the velocity field.

Equation (52) generalizes the mass balance equation (34) used in [20] for the determination of the dopant field.

For solving equation (52) we can use the boundary conditions (39), (40) and (41).

Once velocity field in mushy zone is chosen we can solve the boundary value problem (52), (39), (40) and (41) finding the dopant distribution in mushy zone. This dopant distribution adjacent to the melt/solid interface is a more refined approach of the real dopant field in this region.

1.5 Stability and segregation

Solving boundary value problems (33), (39), (40), (41) or (52), (39), (40) and (41) we obtain dopant distributions which are maybe in a better agreement with experimental data and reflect the real radial segregation. **But the main question, which rests to be solved, is: in which way we can obtain in a steady state regime a semiconductor crystal without radial segregation?**

In our opinion in order to obtain in a steady state regime a semiconductor crystal without radial segregation, the dopant concentration in the mushy zone must be independent on t , x_1 , x_2 . In this sense see also [66] concerning experiments conducted on board LDLG vehicles: "the dopant field close to the growing surface must be uniform prior to low-g growth". A dependence on x_1 , x_2 may lead to segregation. This means that in mushy zone the concentration c of the dopant may depend only on x_3 , $c = c(x_3)$.

Using this kind of functions in the dopant transport equation we find that c satisfies the equation.

$$(53) \quad \pi_Y \cdot D_{33} \cdot \frac{d^2 c}{dx_3^2} = \langle v_3 \rangle \cdot \frac{dc}{dx_3}.$$

Now if $\langle v_3 \rangle$ depends on x_1 and x_2 then equation (38) has only constant solutions. This means that in the mushy zone we must have a constant concentration of the dopant. This corresponds to the Griffin and Motakef recommendation made in [66] but does not satisfy the boundary condition (39). If $\langle v_3 \rangle$ depends only on x_3 we have several solutions for the equation (53) and to each of these corresponds a dopant distribution in mushy zone,

without radial segregation. Obviously we must choose solution which satisfies boundary condition (39), (40) and (41).

In particular if in mushy zone we have $K_{ij} = 0$ for $i \neq j$ and $\partial p^0 / \partial x_3 = 0$ then $\langle v_3 \rangle = 0$ and we have

$$(54) \quad c_0(x_3) = k_1 + k_2 x_3$$

where k_1, k_2 are two constants to be found from (39) and (41). The boundary condition (40) is satisfied for any constants k_1 and k_2 .

If in a steady state regime the dopant concentration in mushy zone is given by a solution of equation (53) then this rests the same all the time, till the regime does not change and we will obtain a semiconductor crystal without radial segregation.

Now the main question is: starting from a certain steady state regime and from the corresponding dopant distribution in which "way" we succeed to realize a new steady state for which the dopant distribution is given by a solution of equation (53)?

In order to give a partial answer to this question we will try to explore the region of attraction (region of stability) of a solution of equation (53). This means that for a solution $c_0 = c_0(x_3)$ of equation (53) we search perturbations which tend to 0 for t tending to $+\infty$. If, for a solution c_0 , the class of this kind of perturbations is sufficiently large then we can try to find a perturbation such that the sum of $c_0 = c_0(x_3)$ and the perturbation at $t=0$ coincides with the dopant distribution corresponding to the starting steady state. If we succeed to find such a perturbation then we have found the "way".

For the beginning, we consider perturbation of the form

$$(55) \quad c_1(x_1, t) = c_1(x_1) e^{\sigma t}$$

and we replace c in the transport equation (25) by

$$(56) \quad c = c_0(x_3) + c_1(x_1) \cdot e^{\sigma t}.$$

We find that $c_1 = c_1(x_1)$ satisfies the equation

$$(57) \quad \sigma \cdot c_1 + \frac{1}{\pi_Y} \langle v_1 \rangle \cdot \frac{dc_1}{dx_1} = D_{11} \cdot \frac{d^2 c_1}{dx_1^2}.$$

If $\langle v_1 \rangle$ depends on x_2 and x_3 then $c_1 = 0$ is the only solution of equation (57). But $c_1 = 0$ is not a real perturbation. If $\langle v_1 \rangle$ depends only on x_1 then equation (57) has several solutions. In particular, for any real σ and $\varepsilon > 0$ equation (57) has solutions with the following property:

$$(58) \quad \sup |c_1(x_1)| < \varepsilon$$

where the supremum is considered on the domain $0 \leq x_1 \leq R$. This means that the above considered solution $c_0 = c_0(x_3)$ is not stable with respect to any perturbation of the form (55).

If we impose to the perturbation (55) to satisfy the boundary condition (40) then we obtain

$$(58) \quad \frac{dc_1}{dx_1} = 0 \quad \text{for } x_1 = 0 \text{ and } x_1 = R.$$

For the Sturm-Liouville problem (57), (58) there exist σ_n and c_{1n} such that $0 > \sigma_1 > \sigma_2 > \sigma_3 > \dots > -\infty$, $c_{1n} = c_{1n}(x_1) \neq 0$ and σ_n, c_{1n} satisfy (57), (58). This means that the concentration profile c_0 defined by (53) is asymptotically stable with respect to the perturbation

$$(59) \quad c_{1n}(x_1, t) = c_{1n}(x_1) e^{\sigma_n t}.$$

Now if we study the stability of the same concentration profile with respect to a perturbation of the type

$$(60) \quad c_2(x_2, t) = c_2(x_2) \cdot e^{\sigma t}$$

we can establish similar facts.

If we investigate the stability of the concentration profile with respect to a perturbation of the type

$$(61) \quad c_{12}(x_1, x_2, t) = c_{12}(x_1, x_2) \cdot e^{\sigma t}$$

we will find other perturbations with respect to which the dopant concentration profile $c_0 = c_0(x_3)$ is asymptotically stable.

This stability results prove that there are time dependent regimes for which the dopant distribution in mushy zone tends to a steady dopant distribution profile without radial segregation. This kind of facts are encouraging but don't mean great things until we have not find the whole family of

perturbations with respect to which the dopant concentration profile $c_0 = c_0(x_3)$ is asymptotically stable.

1.6 The optimal boundary control for a solution without radial segregation

Let us consider in the flow domain M (the melt) the natural convection governed by the equations:

$$(62) \quad -\text{Pr} \cdot \nabla^2 \bar{v} + (\bar{v} \cdot \nabla) \bar{v} + \nabla p = -\text{Ra} \cdot \text{Pr} \cdot \theta \cdot \bar{e}_3$$

$$(63) \quad -\nabla^2 \theta + \bar{v} \cdot \nabla \theta = 0$$

$$(64) \quad \nabla \cdot \bar{v} = 0$$

and the dopant dispersion governed by the equation

$$(65) \quad -\text{Pr} \cdot \nabla^2 c + \text{Sc} \cdot \bar{v} \cdot \nabla c = 0.$$

We assume that the boundary conditions are the followings:

$$(66) \quad \bar{v} = 0 \quad \text{on } \partial M$$

$$(67) \quad \frac{\partial \theta}{\partial n} = \alpha(\theta - \tau) \quad \text{on } \partial M$$

(τ is the temperature of surrounding medium)

$$(68) \quad \frac{\partial c}{\partial n} = \gamma \cdot c \cdot n_3 \quad \text{on } \partial M \quad n_3 = \bar{n} \cdot \bar{e}_3.$$

The aim is to find the boundary controls τ , which give us a desired field of concentration c_d uniform in neighborhood of the melt/solid interface. This means to minimize the cost functional defined by

$$(69) \quad J(c, \tau) = \frac{1}{2} \int_M |c - c_d|^2 dx.$$

We will present some results which are related and can be used in order to solve the above boundary control problem.

Abergel and Casas in the paper [67] consider a more general system as (62)-(64) with boundary conditions similar to conditions (66)-(67) and solve

boundary control problems which consist in minimizing turbulence caused by the heat flux on the boundary i.e. to minimize the cost functional $J(\bar{v}, \tau)$, involving the turbulence, defined by

$$(70) \quad J(\bar{v}, \tau) = \frac{1}{2} \int_M |\nabla \times \bar{v}|^2 dx + \frac{N}{2} \int_{\partial M} |\theta - \tau|^2 ds.$$

Capatina and Stavre in [69] consider also a more general system as the system (62)-(64) with the boundary conditions (66)-(67) and solve the boundary control problems which consist to find the control τ which give as a desired field of temperature θ_d ; i.e. to minimize the cost functional:

$$(71) \quad J(\theta, \tau) = \frac{1}{2} \int_M |\theta - \theta_d|^2 dx.$$

In [70] Capatina and Savre give a numerical treatment of the above boundary control problem. Finite element approximation of the optimality system is defined. The convergence of the proposed algorithms for solving the discrete problem is proved. The analysis of the numerical results and their physical meaning are discussed.

Finally Capatina and Stavre in [71] solve an optimal control problem in biconvective flow; "biconvection" being convection caused by a concentration gradient, not by a temperature gradient. They find the mean values α of concentrations which lead to a given concentration field c_d . They consider the cost functional

$$(72) \quad J(\alpha, c) = \frac{1}{2} \int_M |c - c_d|^2 dx + \frac{N}{2} \alpha^2$$

and formulate the optimal control problem as follows:

$$(73) \quad \min \{J(\alpha, c) | (\alpha, c) \in T\}$$

where T is the nonempty, weakly closed set:

$$(74) \quad T = \{(\alpha, c) \in [0, \infty) \times H^1(\Omega) \mid \exists \bar{v} \text{ such that } (\bar{v}, c) \text{ satisfies (62) - (64)}\}$$

The physical relevant term in (72) is $\frac{1}{2} \int_M |c - c_d|^2 dx$ which provides an

estimate of the difference between the component c of (\bar{v}, c) , and a given configuration c_d of concentration.

This result is very interesting in the case of CdZnTe crystal growth for which the solute Rayleigh number is $Ra_s = 2.02 \times 10^8$ (for GeGa the solute

Rayleigh number is $Ra_s=0$) and consequently equation (62) must be replaced by the equation:

$$(75) \quad -Pr \cdot \nabla^2 \bar{v} + (\bar{v} \nabla) \bar{v} + \nabla p = -(Ra \cdot Pr \cdot \theta + Ra_s \cdot Pr \cdot c) \bar{e}_3$$

1.7 Summary and Recommendation

1. By a synthesis of the results concerning the mass transport in porous media we have identified two transport equations (25) and (42) which generalize the connective-diffusive mass transport equation (4) used in [20] and in general for the determination of the dopant field.
2. Locally, in the precrystallization zone, which can be physically localized, equations (25) and (42) describe with more accuracy the dispersion of the dopant due to the structure which already exists in this region and the interaction between complicated global flow patterns and the convective-diffusive mechanism which exists simultaneously in this region. Equation (25) describes the dispersion process when convection and diffusion balance each other, equation (42) describes the process when convection dominates diffusion.
3. Solving numerically boundary value problems (35), (39), (40) and (41) respectively (52), (39), (40) and (41) for Ga in Ge we hope to obtain better agreements, like Chang and Brown in [20], with experimental data, in the case of steady state regime.
4. For this reason we recommend the implementation of this transport equation in M.A.S.T.R.A.P. computational model.
5. It must be noted that equations (25) and (42) do not take into account the interaction of the dopant field with the crystal. A kind of interaction appears just in boundary condition (39). In this context we can think to improve equations (25) and (42) by the addition of a new term which expresses this interaction. Something like the terms which express absorption and reaction in equation of Hornung and Yäger in [52].
6. The stability calculus made for the steady concentration profiles without radial segregation suggests that rotating the ampule around the longitudinal axis we can reduce $\langle v_3 \rangle$ and obtain a quasi Couette flow in mushy zone, reducing in this way the radial segregation.
7. The optimal boundary control calculus is just a beginning and suggest in how way we can reduced the radial segregation.

2. On the determination of the concentration of the solute in the case of crystal growth by hydrothermal method

2.1 Introduction

We consider the prototype vertical hydrothermal system for obtaining quartz single crystals presented in Fig.1.

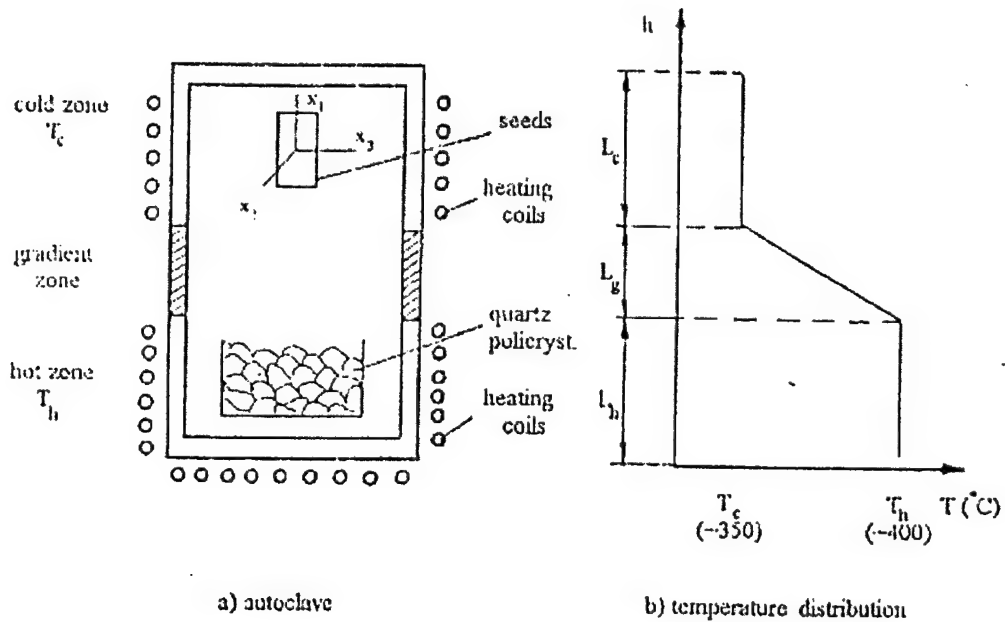


Fig.1. Geometry of the prototype vertical hydrothermal system

Using the transport model of solutes in a porous medium participating in a dissolution reaction in general not in equilibrium; developed by Knaber, Duijn and Hengst in [72]; for the lower region, in the porous bed, if the charge distribution is constant, we find travelling waves. The travelling wave in fact exhibits a sharp dissolution front and is obtained in a nearly explicit manner for two spatially one-dimensional flow regimes with constant water content, bulk density, pore velocity q and diffusion coefficient D . Also for the limit cases of equilibrium reaction or no dispersion, travelling waves are obtained under the same conditions, but with different qualitative properties (see also [73]). It must be noted that the

spatial domain is assumed to be large due to that solutions describe the behavior for large flow domain.

Chen, Prasad, Chatterjee and Larkin in a recent paper [74] since the dissolution and growth process is very slow neglect the effect of dissolution and growth and consider that in the lower region (in porous bed) the flow is a Darcy-Brinkmann-Forchheimer flow model. Their study focuses on the flow and temperature fields without nutrient transport. They use the following nondimensionalized governing equations in the lower region (porous region):

$$(1) \quad \nabla \bar{u} = S_m$$

$$(2) \quad \frac{1}{\varepsilon} \cdot \frac{\partial \bar{u}}{\partial t} + \frac{1}{\varepsilon} (\bar{u} \nabla) \frac{\bar{u}}{\varepsilon} = -\nabla p + Gr \cdot \theta \cdot \bar{e}_3 + \nabla \Lambda \nabla \bar{u} - \left(\frac{1}{Da} + \frac{F_s}{Da} |\bar{u}| \right) \bar{u}$$

$$(3) \quad Se \cdot \frac{\partial \theta}{\partial t} + \bar{u} \cdot \nabla \theta = \frac{1}{Pr} \nabla (R_k \nabla \theta)$$

where: \bar{u} is the dimensionless velocity; S_m the mass source term; ε the porosity; p the dimensionless pressure, $Gr = g \cdot \beta \cdot R^3 \cdot (T_H - T_C) / \nu_f$ is the Grashof number; g the acceleration due to the gravity; β isobaric expansion coefficient; R radius of cylindrical autoclave; T_H and T_C hot and cold temperature; respectively ν_f kinematics viscosity; $\theta = (T - T_C) / (T_H - T_C)$ dimensionless temperature; $\Lambda = \mu_{eff} / \mu$ viscosity ratio; $Da = K / R^2$ Darcy number; K permeability of porous matrix; $F_s = b / R$ Forchheimer number; b Forchheimer coefficient; $Se = (C_p)_{eff} / (C_p)_f$ specific heat ratio; $Pr = (\nu / \alpha)_f$ Prandtl number; $R_k = k_{eff} / k$ ratio of thermal conductivity; α thermal diffusivity.

The flow and temperature dynamic governed by these equations correspond to an isotropic porous media. They develop a three-dimensional algorithm based on the curvilinear finite volume technique and a non-staggered grid layout to simulate the flow and heat transfer in a typical autoclave system. At low Grashof numbers an axisymmetric flow pattern and at high Grashof numbers a three-dimensional flow pattern is predicted. The study is also extended to study the outset of oscillatory flow with a variation in the porous bed height. In the upper region (cold region) Chen, Prasad, Chatterje and Larkin use a system which describe the natural convection without the presence of the seed, governed by the equations:

$$(4) \quad \frac{\partial \bar{v}}{\partial t} + (\bar{v} \nabla) \bar{v} = -\nabla p + \text{Pr} \nabla^2 \bar{v} - \text{Ra} \cdot \text{Pr} \cdot \theta \cdot \bar{e}_1$$

$$(5) \quad \frac{\partial \theta}{\partial t} + \bar{v} \cdot \nabla \theta = \nabla^2 \theta$$

$$(6) \quad \nabla \bar{v} = 0$$

They use the same three-dimensional algorithm based on the curvilinear finite volume technique and a non-staggered grid layout to simulate the flow and heat transfer in the cold region.

These results, for the first time, depict the possible flow patterns in hydrothermal system that can have far reaching consequences on the growth process and crystal quality.

In order to see these consequences it is necessary to consider the nutrient transport equation in homogeneous media:

$$(7) \quad \frac{\partial c}{\partial t} + \frac{\text{Sc}}{\text{Pr}} \cdot \bar{v} \cdot \nabla c = \nabla^2 c$$

and to transpose it in a porous media for the hot zone (lower region of the autoclave) and to analyze the accuracy of equation (7) in the neighborhood of the seed. This analysis is also important because the repartitioning of the nutrient in this zone influence the quality of the grown crystal. In this context the 'diffusion-layer' model introduced by Noyes and Whitney based on a simplified form of equation (7) in the neighborhood of the seed, which importance in crystal growth from solutions has been stressed by Nernst and which was used by several authors for "flat" or "rough" interfaces, it seems to be a "gross oversimplification" of the interaction between complicated flow patterns and solute field. Only detailed calculations of the exact interaction of fluid flow and solute profile adjacent to the interface can be used to estimate the segregation in crystal (see [20]).

Starting from this also for the vertical hydrothermal growth system we propose the substitution of the "stagnant film" or "diffusion layer" by the "precrySTALLIZATION zone" or "mushy zone".

This zone is a thin bed of periodically distributed solid inclusions, which are small with respect to the distance between two neighboring inclusions. The diffusion-layer thickness is substituted by the mushy zone thickness, which can be determined. In this way the diffusion-layer or stagnant film masking the growing crystal is substituted by a thin

periodic porous medium bounded below by an impermeable rigid wall which is the fluid/solid interface.

If the size of solid inclusions is smaller like a critical size (see [23]) the flow in "mushy-zone" is the natural convection given by (4)-(6).

If the size of solid inclusions is critical (see [23]) then the flow in the mushy zone is a Brinkman flow, determined by the global pressure and respecting at the "mushy-zone"/"pure-fluid" interface the Beaves-Joseph or Jones modified Beavers-Joseph or Rudriah conditions (see [24], [25], [26]).

If the size of solid inclusions is larger like the critical size (see [23]) the flow in "mushy-zone" is a Darcy flow, determined by the global pressure and respecting at the "mushy-zone"/"pure-fluids" interface Rudriah conditions (see [26]).

The dispersion mechanism of the nutrient in mushy zone is due to the diffusion and convection, which exists, simultaneously in this periodic porous medium. The dispersion mechanism takes into account the existence of solid inclusions.

This dispersion mechanism of the nutrient in the neighborhood of the interface is more refined as the dispersion mechanism in diffusion-layer model as well as the dispersion mechanism described by equation (7) and is governed by a new convective-diffusive equation which generalize equation (7). In the new convective-diffusive equation we use the velocity field defined by equation (4)-(6) or the Darcy flow determined by this velocity field and a certain periodic micro-structure similar with the micro-structure of the crystal. We find stationary solutions without segregation for the new convective-diffusive equation and perturbation with respect to this solutions are asymptotically stables. We establish also the controllability of the stationary solutions without segregation.

2.2. Porous media based nutrient transport in hot zone

In the following we will describe an algorithm for the determination of the transport equation of the nutrient in the case when the porous medium in the hot zone is periodic, the solid obstacle is symmetric and convection-diffusion balance each other:

1. Let be L ($L = h_L$, Fig.2. pg.23. paper Chen et al.) the size of the porous medium which is divisible into periodic cubes Ω of dimension ℓ presented on the Fig.2.

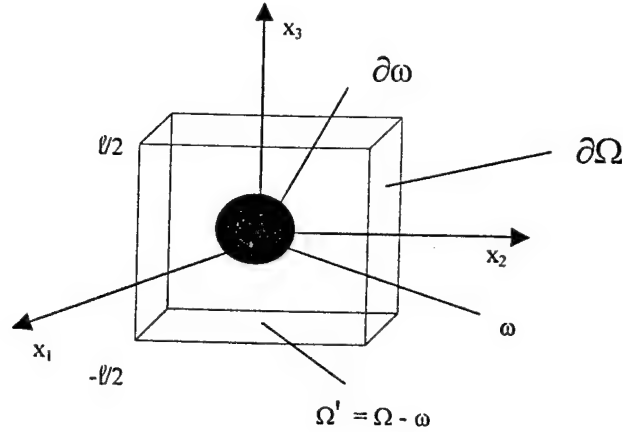


Fig.2.

ω is the solid part; $\Omega' = \Omega - \omega$ is the fluid part; $\partial\omega$ is the boundary of ω ; $\partial\Omega$ is the boundary of Ω .

The solid part ω is assumed to be symmetric with respect to each coordinate plane. It is also assumed that $\varepsilon = \ell/L \ll 1$.

2. In dimensionless variables $y = x/\ell$ this cube is the unite cube Y presented in Fig.3.

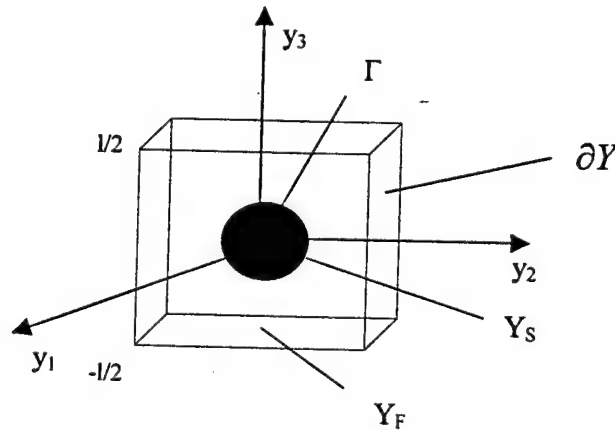


Fig.3.

The fluid domain Y_F and the solid one Y_S have a common smooth boundary Γ .

3. In the unite cube Y we have to solve the following 3-D boundary value problems

$$\begin{aligned} \Delta \chi_i &= 0 & \text{in } Y_F \\ (8) \quad \nabla \chi_i \cdot \bar{n} &= -n_i & \text{on } \Gamma \quad i=1,2,3 \\ \chi_i & \text{ is } Y \text{ periodic} \end{aligned}$$

$$\int_{Y_F} \chi_i dy = 0$$

where: \bar{n} is the external unit normal to the solid boundary Γ ; $\bar{n} = (n_1, n_2, n_3)$; the condition that χ_i is Y periodic means that we have:

$$\begin{aligned} \chi_i(-1/2, y_2, y_3) &= \chi_i(1/2, y_2, y_3) \quad \chi_i(y_1, -1/2, y_3) = \chi_i(y_1, 1/2, y_3) \\ \chi_i(y_1, y_2, -1/2) &= \chi_i(y_1, y_2, 1/2) \quad i=1,2,3. \end{aligned}$$

4. We compute D_{ii}^* defined by

$$(9) \quad D_{ii}^* = D \left(1 + \frac{1}{|Y|} \int_{\Gamma} \chi_i \cdot n_i d\sigma \right) \quad i=1,2,3.$$

5. The nutrient transport equation will be

$$(10) \quad \frac{\partial c}{\partial t} + \frac{1}{\pi_Y} \cdot \nabla c \cdot \bar{v} = \sum_{i=1}^3 D_{ii}^* \cdot \frac{\partial^2 c}{\partial x_i^2}$$

where: $c = c(t, x)$ is the concentration of the nutrient, $\bar{v} = \bar{v}(x)$ is the velocity field of the fluid flow in porous region (find by Chen et al.).

$$\pi_Y = \frac{|Y_F|}{|Y|} \text{ is the porosity.}$$

6. If the solid inclusions are spheres then $D_{11}^* = D_{22}^* = D_{33}^*$.

If the convection is strong and dominate diffusion the above algorithm must be modified as follows:

3'. In the unite cube Y we have to solve the following 3-D boundary value problem:

$$\begin{aligned}
(11) \quad & \mu \Delta_y \bar{v}^j = \nabla_y q^j - \bar{e}_j \quad \text{in } Y_F \\
& \nabla_y \bar{v}^j = 0 \quad \text{in } Y_F \\
& \bar{v}^j = 0 \quad \text{on } \Gamma
\end{aligned}$$

\bar{v}^j and q^j are Y periodic

\bar{e}_j is the unit vector in Y_j direction $j = 1, 2, 3$.

4'. For x in the hot zone we have to compute the velocity field $\bar{v}(x, y)$ defined by

$$(12) \quad \bar{v}(x, y) = - \sum_{j=1}^3 \frac{\partial p}{\partial x_j} \cdot \bar{v}_j$$

where $p = p(x)$ is the pressure field obtained by Chen et al. for this region.

5'. For x in the hot zone we have to take the average $\langle \bar{v} \rangle = \langle \bar{v} \rangle(x)$ defined by

$$(13) \quad \langle \bar{v} \rangle(x) = \frac{1}{|Y|} \int_{Y_F} \bar{v}(x, y) dy.$$

Probably this will be something very close to the velocity field $\bar{v}(x)$ obtained by Chen et al. for the region.

6'. For x in the hot zone we have to solve the following boundary value cell problem

$$\begin{aligned}
(14) \quad & \Delta_y \chi_i - \langle \bar{v} \rangle \cdot \nabla_y \chi_i = v_i - \langle v_i \rangle \quad \text{in } Y_F \\
& \bar{n} \cdot \nabla_y \chi_i = -n_i \quad \text{on } \Gamma \\
& \chi_i \text{ is } Y \text{ periodic} \\
& \int_{Y_F} \chi_i dy = 0
\end{aligned}$$

where: $\langle \bar{v} \rangle = \langle \bar{v} \rangle(x)$ was obtained at 5' -

$v_i = v_i(x, y)$ are the components of $\bar{v}(x, y)$ obtained at 5'

$\chi_i = \chi_i(x, y)$ is unknown.

7'. For x in the hot zone we have to compute D_{ij} defined by

$$(15) \quad D_{ij} = D \left[\delta_{ij} + \frac{1}{|Y|} \int_{\Gamma} \chi_i \cdot n_j d\sigma - \frac{1}{|Y|} \int_{Y_F} v_i \cdot \chi_j dy \right].$$

8'. The transport equation in hot zone will be

$$(16) \quad \frac{\partial c}{\partial t} + \frac{1}{\pi_y} \nabla c \cdot \langle \bar{v} \rangle = \sum_{i=1}^3 \frac{\partial}{\partial x_i} \left(\sum_{j=1}^3 D_{ij} \cdot \frac{\partial c}{\partial x_j} \right).$$

9'. If in hot zone the pressure gradient ∇p is constant then D_{ij} obtained at 7' are constant and in the transport equation obtained at 8' we can use only the symmetric part $D_{ij}^s = \frac{1}{2}(D_{ij} + D_{ji})$ of the diffusion tensor. This symmetric part is given by

$$(17) \quad D_{ij}^s = D \left[\delta_{ij} + \frac{1}{2|Y|} \int_r (\chi_i \cdot n_j + \chi_j \cdot n_i) dy - \frac{1}{2|Y|} \int_{Y_f} (\chi_i v_j + \chi_j v_i) dy \right]$$

and the transport equation becomes

$$(18) \quad \frac{\partial c}{\partial t} + \frac{1}{\pi_Y} \nabla c \cdot \langle \bar{v} \rangle = \sum_{i=1}^3 \sum_{j=1}^3 D_{ij}^s \cdot \frac{\partial^2 c}{\partial x_i \partial x_j}.$$

2.3. The flow in the mushy zone

Thérèse Lévy in the paper [23] studies slow flow of an incompressible viscous fluid in an array of a great number of small fixed particles assuming that the particle size ε and the distance η between two neighbouring solids are such that $\varepsilon \ll \eta \ll 1$. This assumption corresponds to low concentration of solid inclusions. She proves that there exists a critical size for particles, for which Brinkman's law occurs. For larger particle sizes the fluid flow is governed by Darcy's law and smaller sizes solids do not influence the flow.

According to Lévy's paper if in the mushy zone the size of solid inclusions is subcritical then the steady flow in mushy zone is the global convective flow in cold zone defined by the equations:

$$(19) \quad (\bar{v} \nabla) \bar{v} = -\nabla p^0 + \text{Pr} \nabla^2 \bar{v} - \text{Ra} \cdot \text{Pr} \cdot \theta \cdot \bar{e}_1$$

$$(20) \quad \bar{v} \cdot \nabla \theta = \nabla^2 \theta$$

$$(21) \quad \nabla \bar{v} = 0$$

where the Prandtl number Pr and the Rayleigh number Ra are defined by $\text{Pr} = \mu/\alpha_L$, $\text{Ra} = \beta \cdot g(T_h - T_c) \cdot L^3/\alpha_L \cdot \mu$.

If the size of the solid inclusions is critical then the flow in mushy zone is a Brinkman flow governed by a Brinkman's law:

$$(22) \quad \mu \cdot \Delta \langle \bar{v} \rangle = \nabla p^0 + \mu \cdot \varphi \cdot H \cdot \langle \bar{v} \rangle$$

where φ is the volumic concentration of solid particles and H is the translation tensor.

If the size of solid inclusions in mushy zone is super critical then the flow in mushy zone is governed by Darcy's law

$$(23) \quad \mu \cdot \varphi \cdot H \cdot \langle \bar{v} \rangle = -\nabla p^0.$$

We note that in subcritical case is not necessary to put coupling conditions but in supercritical case is absolutely necessary to put this kind of condition in order to realize the continuity of the velocity field. In this order we can use Beavers-Joseph postulate and Rudraiah slip conditions (see [24], [25], [26]).

Once global velocity field \bar{v} and pressure field p^0 are determined from equations (19), (20), (21), in super critical case we use the pressure field p^0 to find, with formula (23), the Darcy's flow $\langle \bar{v} \rangle$. With the above Darcy's flow and the global velocity field \bar{v} using Rudraiah slip conditions at the mushy zone/pure fluid interface we find the small distance d away from this interface in porous side where we make the coupling between the global flow \bar{v} and Darcy's flow $\langle \bar{v} \rangle$.

As following assume that the mean flow in mushy zone is directed along the x_1 axis. This means that $\langle v_1 \rangle \neq 0$ and $\langle v_2 \rangle = \langle v_3 \rangle = 0$.

2.4 The transport equation of the nutrient in mushy zone when convection and diffusion balance each other

Using homogenization method we can obtain the following transport equation for the solute in mushy zone

$$(24) \quad \frac{\partial c}{\partial t} + \frac{1}{\pi_Y} \sum_{i=1}^3 \langle v_i \rangle \cdot \frac{\partial c}{\partial x_i} = \sum_{i=1}^3 \sum_{j=1}^3 D_{ij} \cdot \frac{\partial^2 c}{\partial x_i \partial x_j}.$$

In this equation $c = c(t, x)$ is the solute concentration, $\langle v_i \rangle = \langle v_i \rangle(x)$, $i = 1, 2, 3$ are the components of the fluid velocity in mushy zone given by (19)-(21) or (22) or (23) and D_{ij} are the components of the dispersion tensor. It is understood that equation (24) concerning the case when convection and diffusion balance each other and π_Y is the porosity related to the volumic concentration φ of solid particles by the relation $\pi_Y = 1 - \varphi$.

For symmetric solid inclusions we have

$$(25) \quad D_{ij} = D \left(1 - \varphi + \frac{\varphi}{|y_s|} \int_{\Gamma} \chi_i \cdot n_i d\sigma \right) \delta_{ij}$$

where the functions χ_i are solutions of the Neumann problem

$$(26) \quad \Delta \chi_i = 0 \text{ in } R^3 \setminus Y_s$$

$$(27) \quad \nabla \chi_i \cdot \bar{n} = -n_i \text{ on } \Gamma$$

$i = 1, 2, 3$ (see [53]).

Steady state solutions of equation (24) are given by

$$(28) \quad \frac{1}{\pi_y} \sum_{i=1}^3 \langle v_i \rangle \cdot \frac{\partial c}{\partial x_i} = \sum_{i=1}^3 \sum_{j=1}^3 D_{ij} \frac{\partial^2 c}{\partial x_i \partial x_j}.$$

This equation generalizes the steady state mass balance equation

$$(29) \quad \frac{Sc}{Pr} (\bar{v} \nabla \tilde{c}) = \nabla^2 \tilde{c}$$

used for the determination of the solute field.

In equation (29) Sc represent the Schmidt number $Sc = \mu/D$ and Pr the Prandtl number $Pr = \mu/\alpha_L$.

Boundary condition for solving equation (28) can be formulate starting from the location of the mushy zone. We will assume that the crystal is located in the region $\Omega_1 = [-L_1/2, L_1/2] \times [-L_2/2, L_2/2] \times [-L_3/2, L_3/2]$, the $\pm x_3$ direction is the growth direction and the mushy zones are located in $\Omega_1^+ = [-L_1/2, L_1/2] \times [-L_2/2, L_2/2] \times [L_3/2, (L_3/2) + \delta]$ and $\Omega_1^- = [-L_1/2, L_1/2] \times [-L_2/2, L_2/2] \times [(-L_3/2) - \delta, -L_3/2]$.

For symmetrical reasons we will consider only a part of the mushy zone Ω_1^+ and we will assume that we have

$$(30) \quad \frac{\partial c}{\partial x_3} = \frac{Pe \cdot Sc}{Pr} (1 - k) \cdot c$$

for $x_3 = L_3/2$ and $(x_1, x_2) \in [-L_1/2, L_1/2] \times [-L_2/2, L_2/2]$

which express conservation of mass at the fluid/crystal interface.

On the rest of the boundary of the mushy zone Ω_1^+ we put a coupling condition between the concentration field c defined by (28) and the concentration field \tilde{c} defined by (29) assuring the continuity.

Once the velocity field in mushy zone is determined we can find the concentration field c satisfying equation (28) and the above boundary conditions. This nutrient transport equation in the neighborhood of the

crystal is a new more refined approach of the real nutrient transport in the region.

2.5 The transport equation of the nutrient in mushy zone when convection dominates diffusion

In the case when convection dominates diffusion and the pressure field has constant gradient in mushy zone we have the following transport equation for the solute:

$$(31) \quad \frac{\partial c}{\partial t} + \frac{1}{\pi_Y} \sum_{i=1}^3 \langle v_i \rangle \cdot \frac{\partial c}{\partial x_i} = \sum_{i=1}^3 \sum_{j=1}^3 D_{ij} \cdot \frac{\partial^2 c}{\partial x_i \partial x_j}$$

(see [67]). In this case the components of the dispersion tensor depend also on the velocity field.

If the mean flow is directed along the x_1 axis, what was assumed, then D_{ij} is diagonal with two independent components, that are the longitudinal D_L and transversal dispersivities D_T ; $D_L = D_{11}$ and $D_T = D_{22} = D_{33}$. In the case of small concentration of spheroid solid inclusions Mauri in [75] obtained the following numerical results:

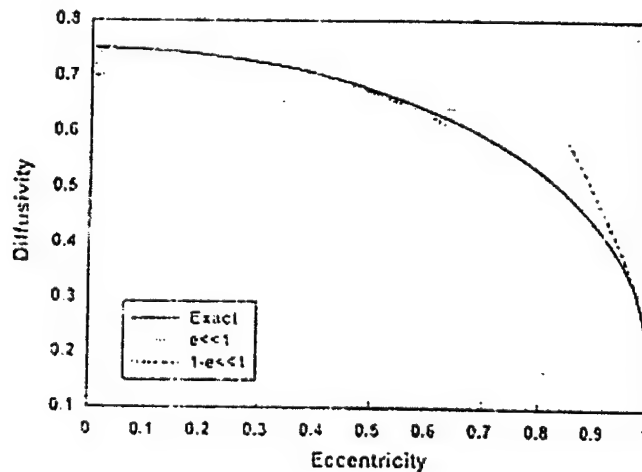


Fig.4a. Longitudinal diffusivity in fixed beds of prolate spheroids as a function of the eccentricity

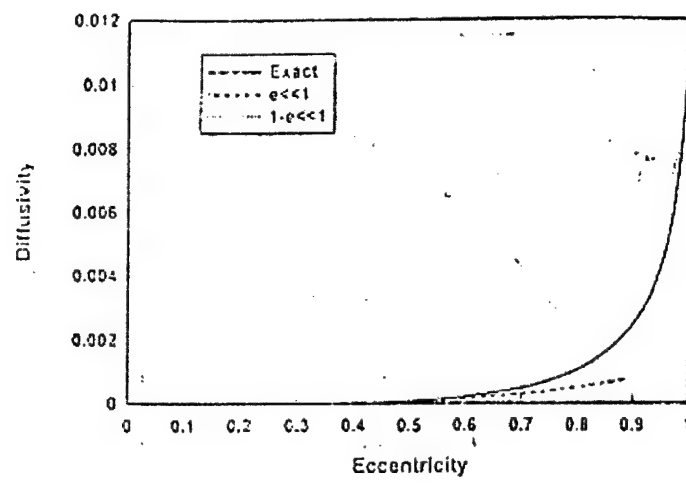


Fig.4b. Transversal diffusivity in fixed beds of prolate spheroids as a function of the eccentricity

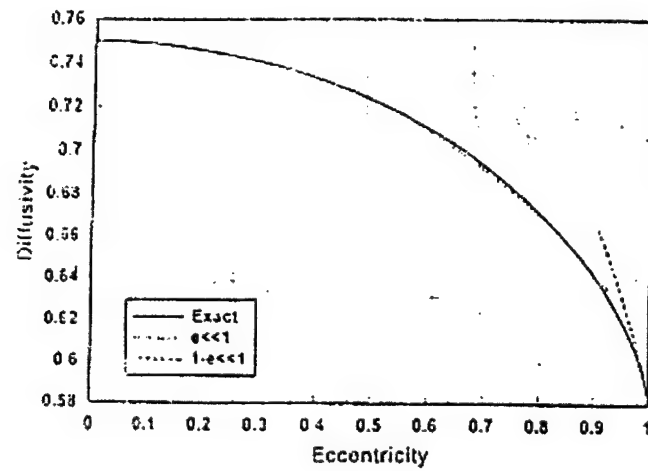


Fig.5a. Longitudinal diffusivity in fixed beds of oblate spheroids as a function of the eccentricity

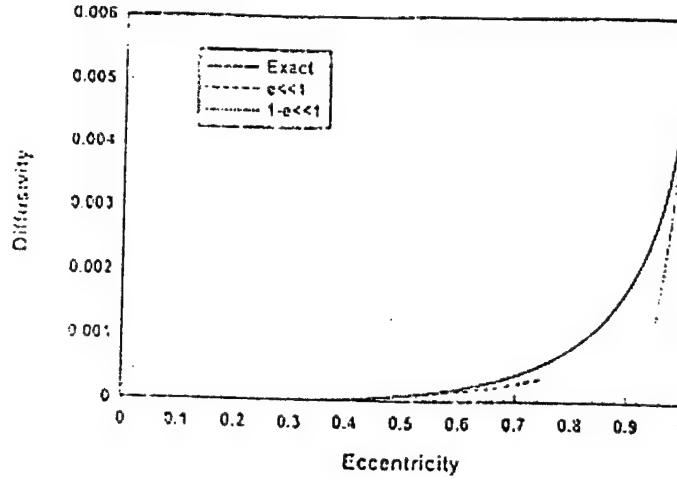


Fig.5b. Transversal diffusivity in fixed beds of oblate spheroids as a function of the eccentricity

Also Mauri in [60] finds analytically for a dilute lattice of uniform spheres that D_T is proportional to $(Pe)^2$ for small Pe and is eight time smaller than D_L .

Therefore in our case equation (31) becomes

$$(32) \quad \frac{\partial c}{\partial t} + \frac{1}{\pi_Y} \cdot \langle v_1 \rangle \cdot \frac{\partial c}{\partial x_1} = D_L \cdot \frac{\partial^2 c}{\partial x_1^2} + D_T \left(\frac{\partial^2 c}{\partial x_2^2} + \frac{\partial^2 c}{\partial x_3^2} \right)$$

Steady state solutions of equation (32) are given by

$$(33) \quad \frac{1}{\pi_Y} \langle v_1 \rangle \cdot \frac{\partial c}{\partial x_1} = D_L \cdot \frac{\partial^2 c}{\partial x_1^2} + D_T \left(\frac{\partial^2 c}{\partial x_2^2} + \frac{\partial^2 c}{\partial x_3^2} \right)$$

Equation (33) generalizes the mass balance equation (29) used for the determination of the solute field.

Equation (33) can be solved using the same boundary conditions like for the equation (28).

Once velocity field in mushy zone is determined we can find the concentration field c satisfying equation (33) and the corresponding boundary conditions.

2.6 Stability and segregation

For obtaining a single crystal in a steady state regime, the solute quartz concentration in the precrystallization zone must be independent on t , x_1 , x_2 . An important dependence on these variables may lead to a dendritic growth. This means that in the neighborhood of the seed the concentration c of the quartz may depend only on x_3 . Using this type of function in equation (33) we find that c satisfies

$$(34) \quad D_T \cdot \frac{d^2 c}{dx_3^2} = 0.$$

The general solution of equation (34) is

$$(35) \quad c_0(x_3) = K_1 + K_2 x_3$$

where K_1 , K_2 are constants.

The constant K_2 is determined by the boundary condition (30) and satisfies

$$(36) \quad K_2 = \frac{Pe \cdot Sc}{Pr} (1-k) \cdot (K_1 + K_2 \cdot L_3 / 2)$$

Therefore we have

$$(37) \quad K_2 = \frac{\frac{Pe \cdot Sc}{Pr} (1-k)}{1 - \frac{L_3}{2} \cdot \frac{Pe \cdot Sc}{Pr} (1-k)} \cdot K_1$$

and

$$(38) \quad c_0(x_3) = K_1 \cdot \left[1 + \frac{\frac{Pe \cdot Sc}{Pr} (1-k)}{1 - \frac{L_3}{2} \cdot \frac{Pe \cdot Sc}{Pr} (1-k)} \cdot x_3 \right].$$

We will analyse the stability of a solute quartz distribution in mushy zone defined by (34). This means that for (38) we search perturbations which tend to 0 for t tending to $+\infty$. The reason is to find time dependent regimes which are able to connect a given dopant distribution in mushy zone with the distribution (38).

For the beginning we consider perturbations of the form

$$(39) \quad c_1(x_1, t) = c_1(x_1) e^{\sigma t}.$$

Substituting (39) in (32) we find

$$(40) \quad D_L \frac{d^2 c_1}{dx_1^2} - \frac{1}{\pi_Y} \langle v_1 \rangle \cdot \frac{dc_1}{dx_1} - \sigma c_1 = 0$$

and we find that $c_0(x_3)$ given by (38) is not stable with respect to any perturbation of the form (39).

If we impose to $c_1(x_1)$ the condition

$$(41) \quad c_1(-L_1/2) = c_1(L_1/2) = 0$$

then we obtain the following inequality for σ :

$$(42) \quad \sigma < -\frac{\langle v_1 \rangle^2}{4(\pi_Y)^2 D_L}.$$

From (40) and (41) we obtain also that

$$(43) \quad c_1^n(x_1, t) = K_1^n \cdot \sin\left(\frac{2n\pi}{L_1} x_1\right) e^{\alpha_1 \cdot x_1} \cdot e^{\sigma_n \cdot t} \quad n = 1, 2, 3, \dots$$

where σ_n is given by

$$(44) \quad \sigma_n = -\frac{1}{4 \cdot D_L} \left[\frac{\langle v_1 \rangle^2}{(\pi_Y)^2} + \frac{16 \cdot D_L^2 \cdot \pi^2 \cdot n^2}{L_1^2} \right] \quad n = 1, 2, 3, \dots$$

and α_1 is given by

$$(45) \quad \alpha_1 = \frac{\langle v_1 \rangle}{2 \cdot \pi_Y \cdot D_L}.$$

The concentration profile defined by (38) is asymptotically stable with respect to the perturbations (43). More than that, these solute quartz distributions are asymptotically stable with respect to the perturbations of the form $c_1 = c_1(x_1, t)$, which satisfy the perturbation equation

$$(46) \quad \frac{\partial c_1}{\partial t} + \frac{1}{\pi_Y} \langle v_1 \rangle \cdot \frac{\partial c_1}{\partial x_1} = D_L \cdot \frac{\partial^2 c_1}{\partial x_1^2}$$

and has the property that at the initial moment $t = 0$ could be expanded as:

$$(47) \quad c_1(x_1, 0) = \sum_{n=1}^{\infty} K_n \cdot \sin\left(\frac{2n\pi}{L_1} x_1\right) \cdot e^{\alpha_1 \cdot x_1}.$$

Next we study the stability of the quartz distribution given by (38) with respect to perturbations of the form

$$(48) \quad c_2(x_2, t) = c_2(x_2) \cdot e^{\sigma t}.$$

In this case is also stands that the distribution $c_0 = c_0(x_3)$ given by (38) is not stable with respect to any perturbation of the form (48).

But if we impose again the spatial periodicity

$$(49) \quad c_2(-L_2/2) = c_2(L_2/2) = 0$$

it turns that the concentration profiles $c_0 = c_0(x_3)$ given by (38) are asymptotically stable with respect to the perturbations:

$$(50) \quad c_2^n(x_2, t) = K_2^n \cdot \sin\left(\frac{2n\pi}{L_2} x_2\right) \cdot e^{\sigma_n t}$$

where σ_n are given by

$$(51) \quad \sigma_n = -\frac{4 \cdot \pi^2 \cdot n^2}{L_2^2} \cdot D_T.$$

The stability with respect to the perturbation of the form

$$(52) \quad c_3(x_3, t) = c_3(x_3) \cdot e^{\sigma t}$$

is treated on a similar manner, reaching the conclusion that there are asymptotically stable with respect to the perturbations:

$$(53) \quad c_3^n(x_3, t) = K_3^n \cdot \sin\left[\frac{2n\pi}{L_3}(x_3 - h + L_3/2)\right] \cdot e^{\sigma_n t}$$

where σ_n are given by

$$(54) \quad \sigma_n = -\frac{4\pi^2 n^2}{L_3^2} \cdot D_T$$

and h is the thickness of the mushy zone.

If we investigate the stability of the solute quartz distribution given by (38) with respect to the perturbation of the form

$$(55) \quad c(x_1, x_2, t) = c_{12}(x_1, x_2) \cdot e^{\sigma t}, \text{ which satisfies}$$

$$(56) \quad c_{12}(-L_1/2, x_2) = c_{12}(L_1/2, x_2) = c_{12}(x_1, -L_2/2) = c_{12}(x_1, L_2/2) = 0$$

we find that the distribution $c_0 = c_0(x_3)$ given by (38) is asymptotically stable with respect to the perturbations:

$$(57) \quad c_{mn}(x_1, x_2, t) = K_1^m \cdot K_2^n \cdot \sin\left(\frac{2m\pi}{L_1} x_1\right) \cdot \sin\left(\frac{2n\pi}{L_2} x_2\right) \cdot e^{\alpha_1 x_1} \cdot e^{\sigma_{mn} t}$$

where σ_{mn} are given by

$$(58) \quad \sigma_{mn} = -\frac{1}{4D_L} \left[\frac{<v_1>^2}{\pi_Y^2} + \frac{16\pi^2 \cdot m^2 \cdot D_L^2}{L_1^2} \right] - \frac{4\pi^2 n^2}{L_2^2} D_T.$$

Finally, if we investigate the asymptotic stability of the quartz distribution $c_0 = c_0(x_3)$ given by (38) with respect to a perturbation of the form

$$(59) \quad c(x_1, x_2, x_3, t) = c(x_1, x_2, x_3) \cdot e^{\sigma t}$$

we conclude that they are asymptotically stable with respect to the perturbation

$$(60) \quad c(x_1, x_2, x_3, t) = K_1^l \cdot K_2^m \cdot K_3^n \cdot \sin\left(\frac{2\ell\pi}{L_1} x_1\right) \cdot \sin\left(\frac{2m\pi}{L_2} x_2\right) \cdot \sin\left[\frac{2n\pi}{L_3} (x_3 - h + L_3/2)\right] e^{\alpha_1 \cdot x_1} \cdot e^{\sigma_{lmn}}$$

where σ_{lmn} are defined by:

$$(61) \quad \sigma_{lmn} = -\frac{1}{4D_L} \left[\frac{\langle v_1 \rangle^2}{\pi_Y^2} + \frac{16\pi^2 \ell^2 D_L^2}{L_1^2} \right] - \frac{4\pi^2 m^2}{L_2^2} \cdot D_T - \frac{4\pi^2 n^2}{L_3^2} \cdot D_T.$$

The stability results obtained till now, could create the impression that the distribution $c_0(x_3)$ given by (38) is stable with respect to any perturbation. For the reason for which we make this study this would be good but unfortunately this is not true. We showed that, generally speaking, for any $\sigma > 0$ and $\varepsilon > 0$ there exists a perturbation $c_1(x_1, t) = c_1(x_1)e^{\sigma t}$ such that for $t = 0$ we have $\sup |c_1(x, 0)| < \varepsilon$. In fact, this was the reason why we have reduced the family of the perturbation of the form $c_1(x_1, t) = c_1(x_1)e^{\sigma t}$ and we have considered only perturbations for which we have $c_1(-L_1/2) = c_1(L_1/2) = 0$. It must be noted that the vanishing condition of $c_1 = c_1(x_1)$ in $-L_1/2$ and $L_1/2$ could not be substituted only by a periodicity condition.

In the problem of the stability of the solute quartz distribution $c_0 = c_0(x_3)$ with respect to perturbations of the form (55), the vanishing condition on the margins $|x_2| = L_2/2$ ($c_{12}(x_1, -L_2/2) = c_{12}(x_1, L_2/2) = 0$) can be replaced with a periodicity condition $c_{12}(x_1, -L_2/2) = c_{12}(x_1, L_2/2)$, but we must conserve the vanishing condition on the margins $|x_1| = L_2/2$ ($c_{12}(-L_2/2, x_2) = c_{12}(L_2/2, x_2) = 0$).

In a similar way we can prove that the quartz distribution $c_0 = c_0(x_3)$ given by equation (38) is asymptotically stable with respect to the following perturbations:

$$(62) \quad c_{n,\lambda,\gamma}(x_1, x_2, t) = K_1^n \cdot \sin\left(\frac{2n\pi}{L_1} x_1\right) e^{\alpha_1 x_1} \cdot \gamma \left[\operatorname{sh} \frac{L_2 z_2}{2} e^{z_1 x_2} - \operatorname{sh} \frac{L_2 z_1}{2} e^{z_2 x_2} \right] \cdot \left(\operatorname{sh} \frac{L_2 (z_2 - z_1)}{2} \right)^{-1} \cdot e^{\sigma_{n,\lambda} \cdot t}$$

where $n = 1, 2, 3, \dots, \gamma \in \mathbb{R}', \gamma \neq 0, \lambda \in \mathbb{R}'; \lambda < 0; K_1^n \in \mathbb{R}'$;

$$\lambda > -\frac{1}{4D_L} \left[\frac{\langle v_1 \rangle^2}{\pi_Y^2} + \frac{16\pi^2 D_L^2}{L_1^2} \right]; z_{1,2} = \mp \sqrt{\frac{-\lambda}{D_T}}; \alpha_1 = \frac{\langle v_1 \rangle}{2\pi_Y \cdot D_L};$$

$$\sigma_{n,\lambda} = -\frac{1}{4D_L} \left[\frac{\langle v_1 \rangle^2}{\pi_Y^2} + \frac{16\pi^2 \cdot n^2 \cdot D_L^2}{L_1^2} \right] - \lambda$$

$$(63) \quad c_{n,\gamma}(x_1, x_2, t) = K_1^n \cdot \sin\left(\frac{2n\pi}{L_1} x_1\right) e^{\alpha_1 x_1} \cdot \gamma \cdot e^{\sigma_n t}$$

where $n = 1, 2, 3, \dots, \gamma \in R', \gamma \neq 0; K_1^n \in R'; \alpha_1 = \frac{\langle v_1 \rangle}{2\pi_Y D_L}$

$$\sigma_n = -\frac{1}{4D_L} \left[\frac{\langle v_1 \rangle^2}{\pi_Y^2} + \frac{16\pi^2 \cdot n^2 \cdot D_L^2}{L_1^2} \right]$$

$$(64) \quad c_{n,\lambda,\gamma}(x_1, x_2, t) = K_1^n \cdot \sin\left(\frac{2n\pi}{L_1} x_1\right) e^{\alpha_1 x_1} \cdot \gamma \cdot \left(\cos \frac{\beta_2 L_2}{2}\right)^{-1} \cdot \cos \beta_2 x_2 \cdot e^{\sigma_{n,\lambda} t}$$

where $n = 1, 2, 3, \dots, \gamma \in R', \gamma \neq 0, \lambda \in R'; \lambda > 0; K_1^n \in R';$

$$\lambda \neq \frac{n^2 \pi^2}{L_2^2} D_T; \beta_2 = \sqrt{\frac{\lambda}{D_T}}; \alpha_1 = \frac{\langle v_1 \rangle}{2\pi_Y D_L}$$

$$\sigma_{n,\lambda} = -\frac{1}{4D_L} \left[\frac{\langle v_1 \rangle^2}{\pi_Y^2} + \frac{16\pi^2 \cdot n^2 \cdot D_L^2}{L_1^2} \right] - \lambda.$$

The perturbation (62) corresponding to the value λ_c given by

$$(65) \quad \lambda_c = -\frac{1}{4D_L} \left[\frac{\langle v_1 \rangle^2}{\pi_Y^2} + \frac{16\pi^2 \cdot D_L^2}{L_1^2} \right]$$

is critical in the sense that for the values of λ smaller than λ_c the distribution (38) of the solute quartz is not stable with respect to the perturbations (62).

Also in the case of perturbations of the form $c(x_1, x_2, x_3, t) = c(x_1, x_2, x_3) \cdot e^{\sigma t}$ the vanishing conditions on the boundaries $|x_2| = L_2/2$ and $x_3 = h - L_3/2, x_3 = h$ can be replaced by periodicity conditions, maintaining the vanishing conditions on the boundary $|x_1| = L_1/2$.

2.7 Conclusions

1. We have identified transport equation, which generalizes the convective-diffusive mass transport equation used in general in crystal growth for the determination of the solute field.
2. Locally in mushy zone these equations describe the dispersion of the solute when convection and diffusion balance each other respective when convection dominates diffusion. These equations take into account the structure which already exists in mushy zone, the interaction between complicated global flow patterns and the convective-diffusive dispersion mechanism in this region.
3. Solving numerically these equations we hope to obtain better agreements with experimental data.
4. For this reason we recommend the implementation of these equations in M.A.S.T.R.A.P. computational model.
5. It must be noted that these equations do not take into account the interaction of the solute field with the crystal. From this point of view these equations can be improved.
6. The stability calculus suggests that there are a lot of time dependent regimes, which tend to a steady state uniform distributed concentration profile.
7. The optimal boundary control calculus, presented for Bridgman-Stocbarger growth, suggest in how way we can reduced the segregation in hydrothermal growth system also.

References

1. Burton, J.A., Prim, R.C. and Slichter, W.P.; J. Chem. Phys. 21 (1953) 1987.
2. Wilson, L.O.; J. Crystal Growth 44 (1978) 371.
3. Wilson, L.O.; J. Crystal Growth 44 (1978) 247.
4. Wagner, C.; J. Metals. 6. (1954). 154.
5. Kim, K. M., Wilt, A.F., Lichtensteiger M. and Gabor, H.C. ; J. Electrochem. Soc. 125. (1978). 475.
6. Favier, J.J.; Acta. Met. 29. (1981). 197.
7. Favier, J.J.; Acta. Met. 29. (1981). 205.
8. Holmes, D.E. , Gatos, H.C.; J. Electrochem. Soc. 128. (1981). 429.
9. Clark, P.A. and Wilcox, W.R. ; J. Crystal Growth 50 (1980) 461.
10. Kobayashi, N. , Wilcox; W.R.; J. Crystal. Growth. 59. (1982). 616.
11. Wilcox, W.R. ; unpublished.
12. Harriott, G.M. and Brown, R.A.; J. Fluid Mech. 126 (1983) 269
13. Harriott, G.M. and Brown, R.A.; Interm. J. Heat Mass Transfer
14. Nikitan, S.A., Polezhayev, V.I. and Fedyushkin, A.I.; J. Crystal Growth 52 (1981) 471.
15. Coriell, S.R., Sekerka, F.R.; J. Crystal. Growth. 46. (1979). 47.
16. Coriell, S.R., Boisvert, R.F., Rehm, R.G. and Sekerka, R.F.; J. Crystal Growth 54 (1981) 167.
17. Etouney H.M. and Brown R.A., J. Crystal Growth 58 (1982) 313.
18. Kaljes, J.P, Chin L-Y. and Carlson F.M.; J. Crystal Growth 61 (1983) 473.
19. Etouney H.M. and Brown R.A., J. Appl. Phys.
20. Chang C.J., Brown R.A.; J. Crystal. Growth. 63. (1983). 343.
21. Adornato P.M., Brown R.A.; J. Crystal. Growth. 80. (1987). 155.
22. Tahar, M.B., Modélisation macroscopique des écoulements et des transferts dans un milieu poreux hétérogène: application à la solidification. Thèse de Doctorat: Université Pierre et Marie Curie, 1997
23. Lévy Th.; C.R. Acad. Sc. Paris. t. 292. (23 mass 1981) Série II. 871.
24. Prasad V.; Convechive flow interaction and heat transfer between fluid and porous layer, pg. 563-615. Dept. of. Mechanical Engineering, Columbia University, New York.
25. Jones J.P.; Proc.Cambr. Phil. Soc. 73. 231-238. (1973).
26. Rudraiah N.; Encyclopedia of fluid mechanics
27. Tartar L.; Incompressible fluid flow in a porous medium. Convergence of the homogenization process. in. Non-homogeneous media and Vibration

- Theory. E. Sanchez-Polencia Ed. Lecture Notes in Physics. Vol. 127. Pp. 368-377. Springer-Verlag. Berlin. 1980.
- 28.. Sanchez-Polencia E; Non-homogeneous Media and Vibration Theory in Springer Lecture Notes in Physics vol. 129. 1980.
 29. Wodié J.C.: Contribution à l'étude des milieux poreux par la méthode de l'homogénéization, Thèse de doctorat à l'Université Paris 6 (1992).
 30. Chiang C. Mei, Jean-Luis Auriault, Chion-ON Na.; Some applications of the homogenization theory: Advances in applied mechanics Volume 32. Academic Press 1996.
 31. Cheo K. Lee, Chin-Cheng Sun and Chiang C. Mei. Int. J. Heat Mass transfer, Vol.39., No.4, pp. 661-676, 1996.
 32. Zick A.A., Homsy G.M. (1980) Stokes flow through periodic arrays of spheres. J. Fluid Mech. 115. 13-26.
 33. Poirier, D.R. (Permeability for Flow of Interdendritic Liquid in Columnar-Dendritic Alloys) Met. Trans., 18.B, 245-255 (1987)
 34. Prescott, P.J. and Incropera, F.P. Advances in Heat Transfer, 28, 231-238 (1996)
 35. Prescott, P.J. and Incropera, F.P. Int. J. Heat Mass Transfer, 34(9) 2351-2359 (1987)
 36. Prescott, P.J. and Incropera, J. Heat Transfer, 116, 742-747, 1994
 37. Voller, V.R. and Prakash, C.; Int. J. Heat Mass Transfer, 30(8), 1709-1719 (1987)
 38. Voller, V.R., Brent, A.D. and Prakash, C.; Int. J. Heat Mass Transfer, 32(9) 1719-1731 (1989)
 39. Beckermann, C.; Ph.D. thesis, Purdue University, West Lafayette (1987)
 40. Beckermann, C. and Viskanta, R.; Phys. Chem. Hydrodynamics, 10, 195-213, 1988
 41. Beckermann, C. and Viskanta, R.; Applt. Mech. Rev. 46(1) 1-27 (1993)
 42. Benuon, W.D. and Incropera, F.P. 1987, Int. J. Heat Mass Transfer, 30(10) 2161-2170 (1987)
 43. Yoo, Hoscon and Viskanta R.; Int. J. Heat and Mass Transfer, 35, 2335-2346 (1992)
 44. Sinha, S.K., Sundaranajan, T. and Grag, X.K.; Int. J. Heat and Mass Transfer 35, 2865-2877 (1992)
 45. Schneider, M.C., Beckermann C.; Int. J. Heat Mass Transfer, 38(18) 3455-3473 (1995)
 46. E. Sanchez -Polencia; Nonlinear Analysis, Methods and Appl. Vol.9. no.11. pp. 1243-1254. (1985).
 47. Lévy Th., E. Sanchez-Polencia; Nonlinear Analysis, Methods and Appl., Vol.9. no.11. pp. 1255-1268.

48. Beavers G.S. and Joseph D.D. (1967) *J. Fluid. Mech.* 30, 197-207.
49. Taylor, J.; *J. Fluid Mech.* 49, 327 (1971)
50. Neal G. and Nader W. (1974) *Can. J. Chem. Eng.* 52. 475-478.
51. Ross, S.M.; *A.I.Ch. E. J.*, 29, 840-846 (1983)
52. Hornung U., Jäger W. *J. of diff. eq.* 92. 199-225 (1991).
53. Baltean D., Lévy Th., Balint St.; *L'étude de la dispersion d'un traceur dans un milieu multiporeux*; (1997 unpublished).
54. Baltean D., Lévy Th., Balint St: to appear in *C.R. Acad. Sc. Paris: Soil Mechanics and Porous Media* (1998)
55. Baltean D., Lévy Th., Balint St.; *Dispersion of a solute in periodic porous media*; *Proceedings of the international Conference, Analysis and numerical computations of solutions of nonlinear systems modeling physical phenomena*, University of the West Timișoara, Romania, 19-21 May. 1997.
56. Balint St., Balint A.M., Baltean D., Neculae A.; *Mass transport by convection and diffusion during melt growth of semiconductor crystals in the context of the Bridgman-Stockbarger crystal growth configuration*; *International Conference an Applied nonlinear dynamics near the Millenium*; University of California, Sand Diego, July 6-11. 1997 (unpublished).
57. D.J. Gunn and C. Pryce; *Dispersion in packed beds. Trans. Inst. Chem. Eng.* 47. T.341-T.350 (1969).
58. J. Salles, J.F. Thovert, R. Delamay, L. Prevors, J.L. Auriault and P.M. Adler; *Taylor dispersion in porous media. Determination of the dispersion tensor. Phys. Fluids* 5, 2348-2376 (1993).
59. D.L. Koch, R.G. Cox, H. Brenner and J.F. Brady: *The effect of order on dispersion in porous media. J. Fluid. mech.* 200 173-188 (1989).
60. R. Mauri; *Lagrangian self-diffusion of Brownian particles in periodic flow fields. Phys. Fluids* 7. 275-284 (1995).
61. J.W. Hiby; *Longitudinal and transverse mixing during single-phase flow through granular beds. Proceedings of the Symposium on the Interaction between fluids and particles London 20-22 June pp.* 312-325 (1962).
62. R.J. Blackwell; *Laboratory studies of microscopic dispersion phenomena. Soc. Petroleum. Engrs. J.* 2. 1-8 (1962).
63. F.E. Grane, G.H.F. Gardner: *Measurements of transverse dispersion in granular media. J. Chem. Engrs. Data* 6 (2) 283-287 (1961).
64. E.J. List, N.H. Brooks; *Lateral dispersion in saturated porous media; J. Geophys. Res.* 72 (10) 2531-2541 (1967).
65. E.S. Simpson: *Transverse dispersion in liquid flow through porous media; V.S. Geol. Surv. Prof. Paper* 411-c (1962).

66. P.R. Griffin and S. Motakef: Influence of non steady gravity. Part.II. in Appl. microgravity tech.II.1989.3..
67. Balint St., Balint A.M., Baltean D.G., Neculae A.: The heat and mass transport by convection and diffusion during quartz crystal growth by hydrothermal system in Proceedings of the International Conference, Analysis and numerical computations of solutions of nonlinear systems modeling physical phenomena; pg. 298-310. Timisoara 19-21 May 1997.
- 68.F. Abergel and E. Casas, M.M.A.N. 27, 223 (1993)
69. A. Capatina and R. Stavre, Int. J.Eng.Sci.Vol.34,Nr.1, pp.59-66, 1996
70. A. Capatina and R. Stavre, Int. J.Eng.Sci.Vol.34,Nr.13, pp.1467-1476, 1996
71. A. Capatina and R. Stavre, J.Math. Kyoto Univ. (JM KYAZ) 37-4, 1998 (585-595)
72. P. Knaber, C.J. van Duijn and S. Neugst: an analysis of crystal dissolution fronts in flows through porous media, In Advances in Water Resources 1995
73. A. Balint, D. Baltean- Solitary wave solutions for the equation of one dimensional flow of a polytropic gas through a homogeneous porous medium. Bull. For Appl. Math. of the Technical University of Budapest, 1264/96 (LXXX) pp.268-276.
74. Q.S. Chen; V. Prasad; A. Chatterjee; J. Larkin; Modeling of fluid flow and heat transfer in a hydrothermal crystal growth system; Use of fluid-superposed porous layer theory
75. R. Mauri: Journ. of Eng. Math. 29. 77-89. 1995.